Master thesis : Finite Element Modelling of Different Strengthening Strategies for Reinforced Concrete Deep Beams

Auteur : Vass, Gergely
Promoteur(s) : Mihaylov, Boyan
Faculté : Faculté des Sciences appliquées
Diplôme : Cours supplémentaires destinés aux étudiants d'échange (Erasmus, ...)
Année académique : 2017-2018
URI/URL : http://hdl.handle.net/2268.2/4439

UNIVERSITY OF LIEGE – FACULTY OF APPLIED SCIENCES

Graduation studies conducted for obtaining a Master's degree in Civil Engineering

Finite Element Modelling of Different Strengthening Strategies for Reinforced Concrete Deep Beams

Author:

Vass Gergely

Jury members:

Boyan Mihaylov

Luc Courard

Jean-Marc Franssen

Frédéric Cerfontaine

Academic year 2017-2018

Abstract

Reinforced concrete deep beams are important structural elements, which transmit loads from the upper structure to widely spaced lower supporting elements. By definition, such members have small shear-span-to-depth ratios and their behavior is governed by shear. Because some deep beams have suffered degradation in existing buildings and bridges, Fiber Reinforced Polymer (FRP) or Ultra-High Performance Fiber Reinforced Concrete (UHPFRC) can be used for their retrofit.

The main goal of this thesis is to use advanced nonlinear finite element models in order to understand the behavior of deep beams retrofitted with FRP sheets and UHPFRC layers. For this purpose, general information about the behavior of FRP and UHPFRC is gathered and summarized. The selected approach for modelling is a smeared rotating crack as formulated in the Modified Compression Field Theory for elements subjected to shear.

Nonlinear finite element analyses are performed on selected experimental studies using program VecTor2. The predictions of the finite element models are compared to the test results in order to validate the model. It is shown that the finite element models capture adequately both load-displacement curves and failure loads of the test specimens.

Using the validated models, a parametric study is performed in order to investigate the effect of FRP sheets and UHPFRC layers on the behavior of true-scale deep beams. The variables considered were the shear-span-to-depth ratio, the layout of FRP sheets, the fiber volume ratio and thickness of UHPFRC layers. The results are compared to identify effectiveness of the two retrofitting strategies and conclusions are drawn.

Acknowledgements

First of all, I would like to thank to every jury member and person who takes his or her time to read this thesis.

My greatest thanks goes to my advisor, Professor Boyan Mihaylov, who guided me throughout my work. He always provided me with helpful observations and suggestions during our meetings throughout the whole semester. His mindset of always analyzing the problem thoroughly, several times, never making premature conclusions really helped me to deepen my knowledge in the field of new, novel retrofitting materials. I am greatly indebted to him.

I would like to thank all the help I got from my office colleagues Renaud Franssen, Nikola Tatar and Jian Liu. They never turned me down, when I had questions. It has been a great experience working in such a welcoming environment.

I would like to thank Professor Cristina Campian from my home university, for always helping me. Even though we were in different countries, she always took time to answer my questions.

Finally, I would like to thank my family and my old friends for their support, and my new Erasmus friends for the amazing time spent in Liège.

Contents

List of Figures

List of Tables

1. Introduction

1.1. Context and motivation

In the last century the use of transfer beams rose considerably. Its application extends from high-rise buildings to bridges in every form and from every type of material. Because some structures having transfer beams are past their serviceability time, and degradations have appeared, their retrofit is essential for continuous exploitation.

In order to understand the behavior of transfer beams, one has to define their purpose and the main forces acting within them. As defined by Nie et al. (2017), transfer beams are beams which transmit loads from upper structure to widely spaced lower supporting elements such as columns or walls. Due to the fact that these beams are used in lower parts of the building for architectural purposes or for shopping areas, their size has to be big enough to support the whole upper structure. In some cases these transfer beams can reach up to 2-3 floors height.

Because of their small shear-span-to-depth ratios (a/d<2.5), transfer beams are often considered as deep beam as seen in Figure 1. The main failure loads are not flexural ones, as in the case of slender beams, but shear failures. Their behavior is best modelled through the strut-and-tie approach.

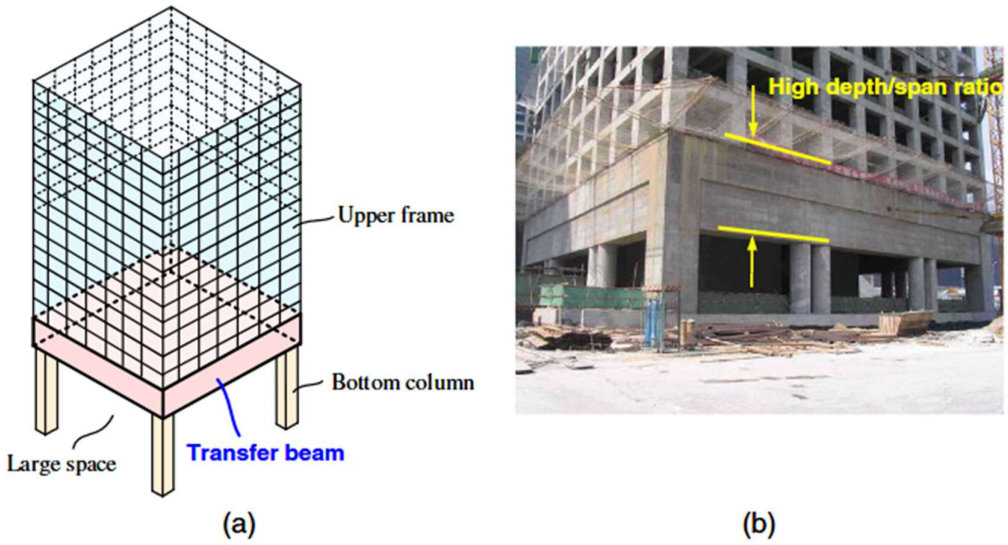

Figure 1. Deep transfer girders in high-rise buildings (Nie et al. 2017)

In the case of bridges, cap beams create the connection between the deck and the columns. Thus their main role is to concentrate the distributed forces into point ones. Their span can vary from 25 to 150m, depending on the traffic on the bridge, the environmental conditions, etc. They are usually made of reinforced concrete.

Retrofitting bridge girders and cap beams can be of great importance due to their essential role in the infrastructure of a country. Many were built more than 60 years ago, thus several have serious degradations. In this thesis their retrofit using Fiber-Reinforced Polymer sheets and Ultra High Performance Fiber-Reinforced Concrete layers will be analyzed and compared.

Figure 2 Deep cap beams in Dunn Memorial Bridge stub end (Wikipedia)

1.2. Objectives of the thesis

In recent times retrofit actions on old buildings being past their service life became imminent. Especially deep beams suffered damage due to constant loading, degradations due to hars environmental conditions, aging etc. For this, use of novel materials such as Fiber-Reinforced Polymers (FRP) and Ultra High Performance Fiber-Reinforced Concrete (UHPFRC) as possible retrofitting options will be tested. For this purpose finite element models will be built in software VecTor2.

The objective of this thesis is to model deep beams retrofitted with FRP and UHPFRC and to predict their behavior, flexural and shear strengths. Also the two retrofit techniques will be compared.

1.3. Outline of the thesis

The thesis consists of 6 chapters, including Chapter 1.

Chapter 2 includes the relevant literature used in the thesis. General information such as properties or advantages and disadvantages concerning the use of FRP and UHPFRC are described. This chapter also specifies the finite element modelling by explaining the theory behind program VecTor2, namely the Modified Compression Field Theory.

Chapter 3 presents the finite element modelling of deep beams strengthened with FRP sheets. Experimental data of FRP-strengthened deep beams from previous tests are presented after which finite element models of the same specimens are described. Finally results are discussed and comparison is made between test specimen and finite element model.

Chapter 4 explains the finite element modelling of deep beams strengthened with UHPFRC. Experimental data of UHPFRC-strengthened deep beams are presented after which finite element models of the same specimens are described. Finally results are discussed and comparison is made between test specimen and finite element model.

Chapter 5 consists of the parametric study and comparison. Several parameters are studied such as span-to-depth ratio and FRP configuration for FRP-retrofitted beams and span-to-depth ratio, fiber volume ratio and layer thickness in case of UHPFRC-retrofitted beams.

Chapter 6 presents the general summary and conclusions of the thesis.

2. Literature review

2.1. Strengthening with Fiber-Reinforced Polymer (FRP) sheets

In recent years, a lot of existing structures are past the service life. Due to this fact, their rehabilitation has been a major concern. The primary reasons for strengthening of structures as described by Malek et al. (1998) include:

- Resistance upgrade to bear underestimated loads
- Changing the structural capacity to withstand higher loads
- Prevent premature failure
- Restoring corroded elements to former load carrying capacity
- Aging, creep and other types of degradations

One of the newer and highly promising materials for retrofitting purpose are the fiber-reinforced polymer (FRP) composites. These can be mainly found in forms of thin unidirectional *strips*, or flexible *sheets* or *fabrics*, having one or at least two orientations of fibers (fib Bulletin No. 14).

Mainly when we are talking about FRP strengthening systems, we have to look at the three main components, which are:

- Adhesives
- Matrices
- Fibers

Different types of FRP products are presented in Figure 3.

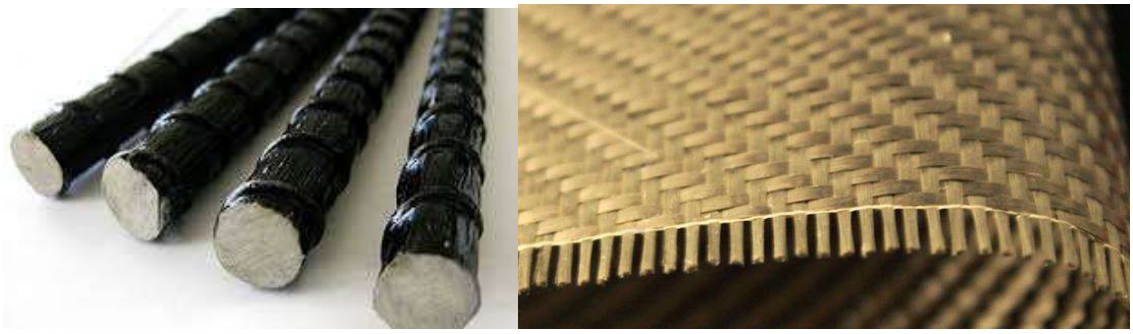

(a) (b)

(c)

Figure 3 Different types of FRP products (a) Carbon FRP rebar, (b) Basalt FRP composite, (c) FRP sheets. (Sourse: Ref nr 9)

2.1.1. Properties of FRP sheets

Components

As mentioned above, FRP strengthening systems have three main components, respectively adhesives, matrices and fibers. Adhesives bind together the concrete and FRP material in order to get a composite action (fib Bulletin No. 14). Because the load transfer is passing through the adhesive layer also, it is important to have necessary shear and bond strengths. One of the most used adhesives is epoxy, due to the fact that it has great strength characteristics and is commonly found. The key to a successful composite action lies on several preparation aspects. Such preparations are namely adherent materials, mixing temperatures, surface preparations etc.

There are two time concepts, when talking about adhesives: *Pot life* and *Open time*. Fib bulletin No. 14 describes Pot life as the amount of time one can work with adhesive after mixing, but before hardening in the vessel, and Open time, which is the amount of time one can utilize to join together the adherent components, after the adhesive has been applied to them. Epoxy adhesives are used also because of long Open time.

The Matrix is the component in which the fibers are embedded and so connected. It also has the important role to protect the fibers against corrosion and to create a bridge between the fibers in order for the loads to be evenly distributed. Main physical and chemical characteristics of these matrices mentioned in fib bulleting No. 14 are melting/curing temperature, viscosity and reactivity with fibers. To have a good connection between the adhesives and the matrices, the latter are also mainly made of epoxy resins or polyester.

Fibers, being the third component, exhibit linear elastic behavior and do not have yield plateau as steel (fib bulletin No. 14). The three main categories of fibers are carbon, glass and aramid. These type of fibers have been studied by Feldman 1989 and Kim 1995. The typical values for Elastic modulus, tensile strength and ultimate strain are presented in table 1.

Material	Elastic modulus (GPa)	Tensile strength (MPa)	Ultimate tensile strain (%)
Carbon			
High strength	215-235	3500-4800	1.4-2.0
Ultra high strength	215-235	3500-6000	1.5-2.3
High modulus	350-500	2500-3100	0.5-0.9
Ultra high modulus	500-700	2100-2400	0.2-0.4
Glass			
E	70	1900-3000	3.0-4.5
S	85-90	3500-4800	4.5-5.5
Aramid			
Low modulus	70-80	3500-4100	4.3-5.0
High modulus	115-130	3500-4000	2.5-3.5

Table 1 Typical properties of fibers (fib Bulletin No. 14)

Stress-strain behavior

Firstly, when the material is transformed into fibrous form, its stiffness and strength is enhanced compared to the bulk form. Also, due to the high length/diameter ratio, the load transfer from the matrix to the fiber is an effective one (fib Bulletin No. 14). This gives FRP composites a high tensile strength. As seen in Figure 4. Carbon FRP-s can have as high as 2000 MPa ultimate strength in tension.

It can also be seen, that unlike steel, which has a bilinear response, FRP sheets behave linear elastically. This phenomenon can be attributed to the fibrous nature, as mentioned above.

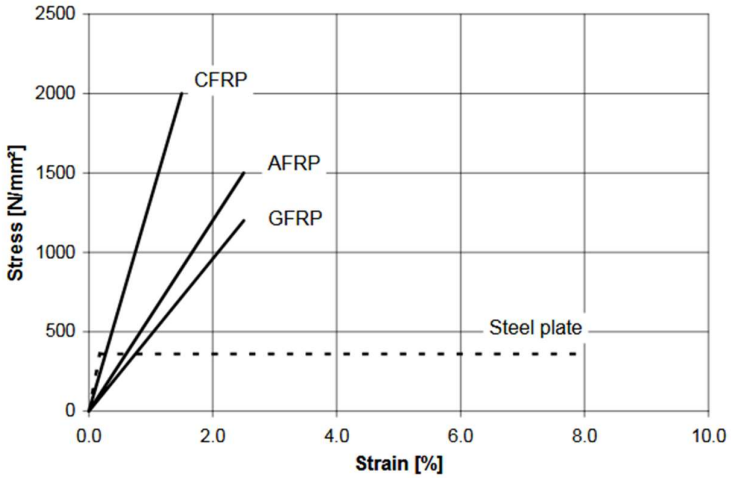

Figure 4 Stress-strain behavior of reinforcement for external bonding (Matthys 2000). CFRP = carbon FRP, AFRP = aramid FRP, GFRP = glass FRP.

Secondly, due to FRP sheets' superior characteristics, the thicknesses of the repairing layers are in the order of few mm. This combination of high strength and low cross sectional area greatly reduce the extra weight added to the structure, and also helps in maintaining aspects

which are close to the initial architectural design. On the other hand, due to the thin layers, the material behaves only in tension, having almost zero compressive strength.

2.1.2. Advantages and disadvantages of FRP sheets

There are several criteria, when selecting a proper strengthening system, namely the condition in which the structure is, environmental conditions, cost effectiveness being the most important one.

Matthys (2000) compared the FRP sheets rehabilitation system with the steel plate bonding one. In the following list are some of the advantages of the FRP sheets:

- Unlike steel, FRP sheets don't need protection against corrosion.
- FRP elements are light weight rehabilitation tools and can be purchased in any kind of dimensions. These factors make them flexible and of easy use. On the contrary, steel plates are heavier, come in predefined dimensions, and when applied in large projects, a proper connection system has to be developed between the plates.
- Since FRP sheets are thinner than steel plates and have a large bond width/thickness ratio, stresses which are produced at the interface of materials are low. Hence in many cases there is no need of mechanical anchorage.
- FRP elements have excellent fatigue behavior.
- Small thickness and lack of mechanical anchorages make FRP sheets aesthetically pleasing. Also different types of finishing layers can be applied.

When comparison of two retrofit systems is made, it is also important to highlight the disadvantages, which for FRP are:

- In comparison to steel, FRP has higher initial cost. CFRP can be at least 6 times more expensive than steel plates. This difference can be reduced by the labour cost and future reparation expenses.
- FRP elements have low transverse strength. This makes FRP sheets more vulnerable to direct impact action. Hence, in some cases, a protective layer has to be added.
- FRP retrofit systems are exposed to high temperatures (e.g. in case of fire), some epoxy resins starting to soften even at low temperatures (45-70°C) (fib bulletin Nr. 14).

All in all, this shows that there are several factors which have to be taken into consideration, when using FRP sheets as retrofitting systems. As future research is made in order to make the material more accessible for the market, so will its use be seen in more structural retrofitting works.

2.2. Strengthening with Ultra High Performance Fiber-Reinforced Concrete (UHPFRC)

Even though the Reinforced concrete was invented and patented in 19th century, it was only in the beginning of the 20th century, that it was used in more and more constructions. Also, the development of high and ultra-high performance materials began 30 years ago (High-Performance Construction Materials, 2008), when a demand rose to retrofit existing concrete structures in order to extend their service lives. Much research has been made in this direction, in order to create more efficient materials with high durability and strength.

When talking about ultra-high performance materials, UHPFRC is one of the major subjects. This novel material is composed of two main components, namely matrix and fibers. In the term matrix are included all the components of the matrix, such as cement, water, aggregates, additives, etc. Fibers are mixed in discontinuous and randomly oriented ways inside the matrix. They are mainly made of steel, carbon or glass. These two components are connected by bonding, hence one major characteristic of UHPFRC is its bond strength. In Figure 5 a test beam retrofitted with UHPFRC is presented.

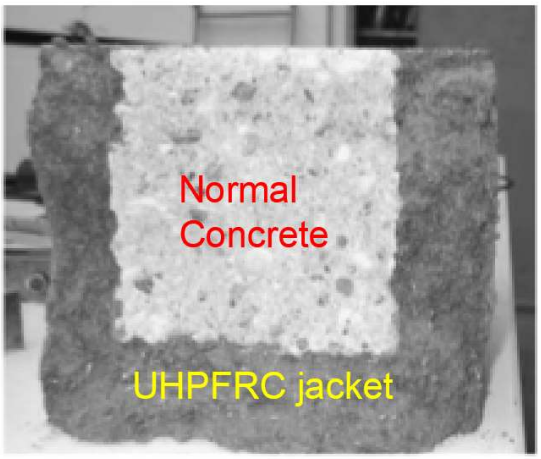

Figure 5 Test beam retrofitted with UHPFRC jacket (Martinola et al. 2010)

2.2.1. Properties of UHPFRC

One can define UHPFRC as a cementitious composite material having compressive strength of over 170 MPa and tensile strength exceeding 8 MPa as described by Tayeh et al. (2013). These high strengths can be obtained due to two major facts, namely preparation mode and fiber content. Under the term preparation mode one can understand the type of cement and size of aggregates used, but also the addition of silica fume or fly ash in some cases in order to reduce the volume of voids in the matrix. Different natural environments require different mixtures in order to obtain the required durability and strength. The second component, namely fibers have an effect on the tensile strength of UHPFRC. These fibers come in different sizes, shapes and

are made of different types of material as mentioned above. The way they work is by creating a miniature bridge across the micro-cracks, to transfer the tension.

An important characteristic of the UPHFRC is its stress-elongation curve in tension. The stress-elongation curve helps differentiate conventional FRC from high-performance one by analyzing its response in the post-cracked stage.

As it can be seen in Figure 6. A.E. Naaman (2007) defined 3 stages of behavior in tension. These stages are the following:

- I. Elastic behavior
- II. Strain-hardening behavior
- III. Strain-softening behavior

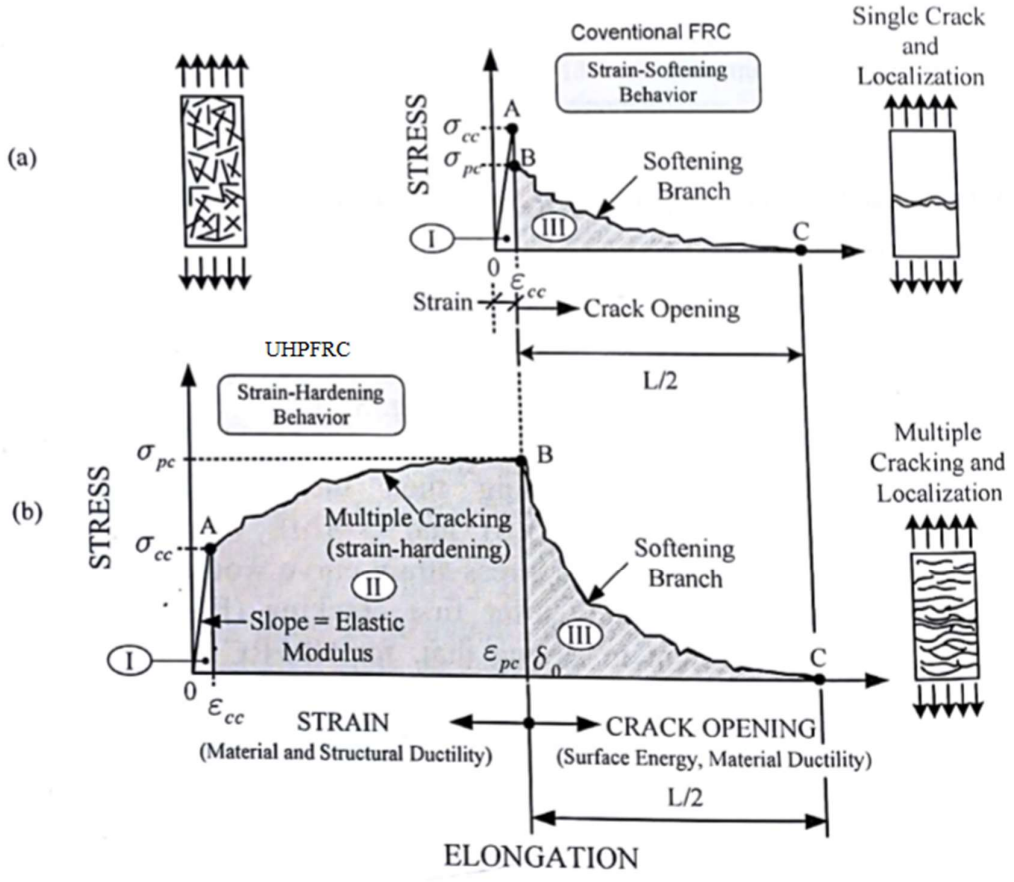

Figure 6 Comparison made by A.E.Naaman (2007) of typical stress-elongation curve in tension (a) Conventional strain-softening FRC. (b) Strain-hardening FRC composite

The first stage can be characterized by a pre-cracking behavior of the concrete. During this stage a linear elastic ascending portion can be noticed until the first-crack stress σ_{cc} is reached.

The second stage consist of the strain-hardening behavior, when multiple micro-cracks develop inside the matrix. Also during this stage a high energy is absorbed. This phenomenon can be attributed to the fact that in high performance FRCs the post-cracking stress σ_{pc} is greater than

the initial cracking stress. The matrix has a tendency to create new cracks instead of enlarging the existing ones.

The final stage commences when the post-cracking stress is reached. The following softening causes reduced strength, and widens a critical crack. Simultaneously, smaller cracks can become narrower, even close.

Zani et al. (2017) studied the size effect of the dog-bone samples when uniaxial tension experiment is conducted. They created 4 samples having the gauge lengths of 20, 80, 200 and 440 mm. It was observed that longer specimens exhibit more brittle behavior and have smaller tensile strengths. In Figure 7 the crack patterns of the samples are displayed.

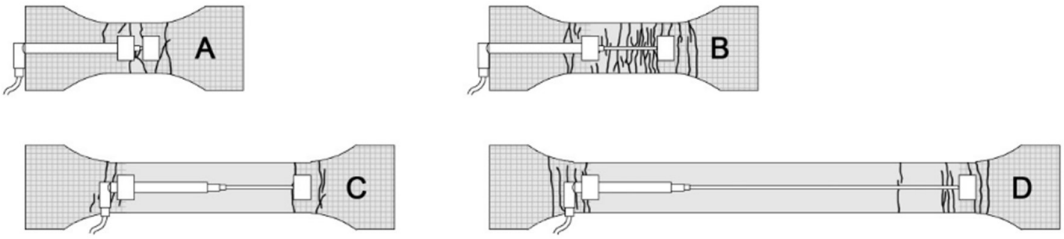

Figure 7 Crack patterns of dog-bone samples (gauge lengths: A-20mm, B-80mm, C-200mm, D-440mm) (Zani et al. 2017)

It can also be noted, that only in test B can multiple cracking be seen. In the longer specimens a crack localization happens, that can be attributed to the change in the dimensions of the samples.

Another important factor which influences the tensile response of UHPFRC materials is the orientation of fibers and the number of fibers which pass through a unit area. Da Silva et al. (2017) made an experiment with Ultra High Performance Fiber-Reinforced Self-Compacting Concrete (UHPFRSCC), where they examined the fiber orientation flow at different heights of the specimens. They found that as the fiber orientation factor, which indicates the number of fibers bridging the crack, closes to 1, so the tensile strength increases.

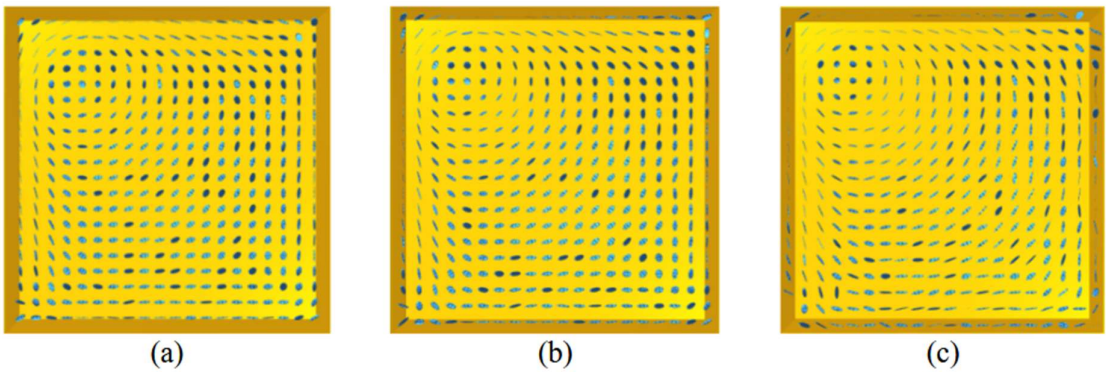

Figure 8 Fiber orientation ellipsoids at different horizontal planes (a) close to the bottom, (b) mid-plane, (c) near the top (Da Silva et al. 2017)

When talking about the compressive strength of UHPFRC, the same parabolic curve is considered as in the case of normal concrete. One main difference that can be noticed was studied by Riedel et al. (2017), namely the effect of specimen shape.

The experiment consisted of a large number of specimens made of Normal Strength Concrete (NSC), High Strength Concrete (HSC) and Ultra High Performance Concrete (UHPC). No fibers were added to the concrete mixes in order not to influence the outcome of the test. As it can be seen in Table 2, the main focus was on the ratios between the cylindrical strength and cubic strength of the materials.

Series	1	2	3	4	5
Type of concrete	NSC d_g = 16 mm	HSC d_g = 16 mm	UHPC d_g = 3 mm	UHPC d_g = 0.5 mm	UHPC d_g = 8 mm
Ratio (Cyl150/Cube100) [-]	0.75	0.83	0.90	0.98	0.98
Ratio (Cyl150/Cube150) [-]	0.79	0.84	0.94	-	-
Ratio (Cyl100/Cube100) [-]	0.78	0.84	0.94	0.98	0.98
Ratio (Cyl150/Cyl100) [-]	0.96	0.99	0.96	1.00	1.00
Ratio (Cube150/Cube100) [-]	0.95	0.99	0.95	-	-

Table 2 Ratio of compressive strength between different specimen sizes (Riedel et al 2017)

where dg= maximum diameter of aggregate.

From the results it can be stated, that in case of UHPC the ratio between cylindrical and cubic strength is almost 1. This means that compressive strength tests can be performed on both specimen types with relatively close results and that UHPC strength classes have to be defined in other ways than that of Normal Concrete ones.

2.2.2. Advantages and disadvantages of UHPFRC jackets

UHPFRC is considered a relatively new material in construction field. Thus many engineers are not yet familiar with its. In the following list are some of the advantages of UHPFRC:

- Compared to normal concrete or even high-strength concrete, UHPFRC exhibits far greater compressive strength, usually above 150 MPa. Thus cross-sections of elements can be reduced.
- Due to fiber content, UHPFRC has considerable tensile strength, when compared to normal concrete.
- UHPFRC has a fast curing time. In the first two days it can reach up to 70% of its ultimate strength. Thus elements can be loaded after 48 hours.
- Due to the composition of UHPFRC, its flowability is greater than of normal concrete. It can be used to fill small spaces without creating voids inside the concrete matrix. Thicknesses are mostly limited by the length of the fibers.
- UHPFRC can be considered an almost impermeable material. This makes the material a perfect protection for steel against corrosion or chemical degradation. Thus structures

using UHPFRC become very durable and have longer service lives than normal concrete ones.

Having presented the advantages of UHPFRC it is also important to highlight its drawbacks, such as:

- Initial costs of structures using UHPFRC is much higher than the ones using normal of high-strength concrete. This can discourage investors in using the material.
- Even though a lot of research was conducted concerning UHPFRC in the last decades, there is still no general design code for structure made out of this material, thus each project needs to be considered individually.
- For now, only a few producers of UHPFRC exist on the market. Also special preparation method of the material is known by only a few specialists.
- Many current engineers do not have enough information about UHPFRC to make them comfortable enough to apply retrofit designs based on the material. Simple and thorough presentations have to be made for them in order for the material to be more promoted in practical field also.

2.2.3. UHPFRC applications: retrofitting

Due to its superior strength and durability, UHPFRC is used more and more in retrofitting old RC and steel structures. Since the early 2000s it was a preferential choice in projects such as rehabilitation of bridges, buildings, maritime signalization structures etc.

In this paragraph a couple of retrofit examples follow:

- *RIBBED SLAB STRENGTHENING IN A BUILDING, GENEVA (Moreillon et al. 2013)*

The building in question was erected in the 1920s, and has a RC slab supported by masonry wall type of setup. Due to requirements for higher load bearing capacity, its retrofit was imminent.

UHPFRC layer of 30 mm with passive reinforcement was proposed as a retrofit design. This approach was selected due to reduced construction time, only small increase in dead load and the ability to neglect foundation strengthening.

The connection between the old slab and the new UHPFRC layer is realized through Gritblasting, as seen in figure 7, thus the roughened surface connects the two layers.

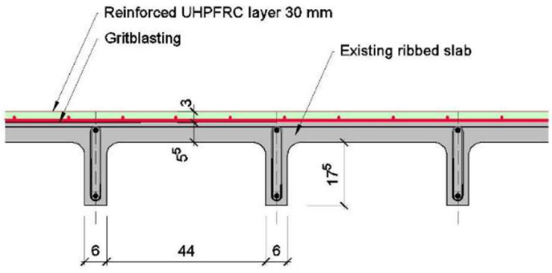

Figure 9 Cross section of the strengthening procedure of the ribbed slab (Moreillon et al. 2013)

- *RETROFIT OF MARITIME SIGNALIZATION TOWER (Denarié et al. 2013)*

In this case intervention was needed due to harsh environmental exposure of the maritime tower. Also due to tidal waves, the access of the tower, which was built about 70 years before, was restricted, sea level differences being almost 5m between low and high tide.

A special formwork was designed for this case, which could withstand the pressure of the liquid UHPFRC and stops any concrete from leaking out as seen in Figure 10.

Figure 10 The formwork being placed on the small island, around the tower (Denarié et al. 2013)

Quickness of application and high durability against salty environment were key factors in using UHPFRC.

- *BRIDGE STRENGTHENING, VUARRENS (Moreillon et al. 2013)*

Many bridges suffer deterioration due to high traffic loading and corrosion of reinforcement due to lack or deficiency in waterproof membranes. These issues can be solved by adding a thin layer of UHPFRC, which offers waterproofing and durability for a long period of time.

The bridge in Vuarrens presents a case mentioned above. This 24.60m long, 10.70m wide bridge has corroded rebars and degraded elements. To rehabilitate it, the old surface was hydrodemolitioned and a new UHPFRC layer of 30 mm thickness was cast over it. Due to the fact that the project was executed in 2 phases in order to reduce the impact on traffic, a joint was realized between the 2 parts using rebars. In figure 9 the detailing of execution is presented.

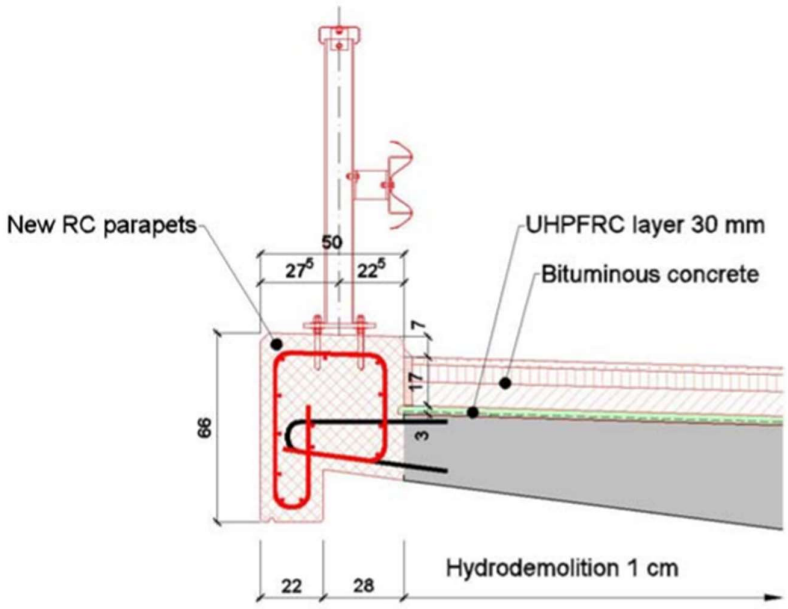

Figure 11 Detail of RC parapet and new UHPFRC layer (Moreillon et al. 2013)

2.3. Finite Element modelling

Modified Compression Field Theory

The finite element modelling program used for the numerical parts of the thesis is VecTor2. It is based on an analytical model called Modified Compression Field Theory (MCFT), developed by Vecchio and Collins (1986).

The MCFT focuses on the complete nonlinear behavior of reinforced concrete panels subjected to in-plane shear and normal stresses. The theory is built on the following main assumptions:

- The reinforcement is uniformly distributed inside the panel
- Smeared rotating cracks which can reorient depending on the principal concrete stresses
- Uniformly applied stresses (both normal and shear ones)
- Perfect bond between concrete and reinforcement
- Reinforcements have only normal stresses
- Within a finite element stresses and strains have average values
- Each strain phase has its unique stress phase

Three sets of equations compose the MCFT, namely compatibility, equilibrium and constitutive relationships.

Compatibility relationships

Looking at Figure 12 one can see the average strains developed in concrete.

Having the assumption of perfect bond between concrete and steel, the strains produced in the two materials are the identical. Defining the equations for the two main directions x and y we get the following equations:

$$\varepsilon_x = \varepsilon_{cx} = \varepsilon_{sx} \quad (2.3.1)$$

$$\varepsilon_y = \varepsilon_{cy} = \varepsilon_{sy} \quad (2.3.2)$$

Having also the value for shear strain, γ_{xy}, using Mohr's circle of strains, one can express the principal concrete tensile and compression strains (ε_{c1}, ε_{c2}).

$$\varepsilon_{c1}, \varepsilon_{c2} = \frac{1}{2}\left(\varepsilon_x + \varepsilon_y\right) \pm \frac{1}{2}\left[\left(\varepsilon_x - \varepsilon_y\right)^2 + \gamma_{xy}{}^2\right]^{\frac{1}{2}} \quad (2.3.3)$$

When determining the principal stress and tensile strain axes we use the following equation:

$$\theta = \theta_\sigma = \theta_\varepsilon = \frac{1}{2}\tan^{-1}\left(\frac{\gamma_{xy}}{\varepsilon_x - \varepsilon_y}\right) \quad (2.3.4)$$

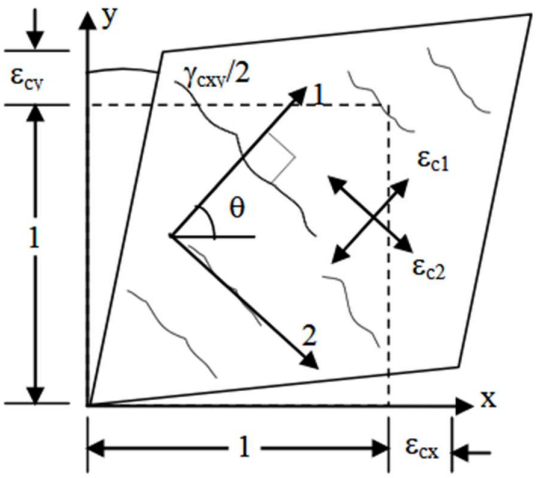

Figure 12 Average concrete strains from stress-strain response (Vecchio 2013)

Equilibrium Relationships

Consider a free body as seen in Figure 13.

When talking about equilibrium, one refers to the balance between the applied stresses (σ_x, σ_y, τ_{xy}) and the average stresses in the concrete and reinforcement (f_{cx}, f_{cy}, f_{sx}, f_{sy}, ν_{cxy}).

These relationships can be defined in the following manner:

$$\sigma_x = f_{cx} + \rho_{sx} f_{sx} \quad (2.3.5)$$

$$\sigma_y = f_{cy} + \rho_{sy} f_{sy} \quad (2.3.6)$$

$$\tau_{xy} = \nu_{cxy} \quad (2.3.7)$$

From the Mohr's circle of stresses, one an also express:

$$f_{cx} = f_{c1} - \nu_{cxy} \cot(90 - \theta_\sigma) \quad (2.3.8)$$

$$f_{cy} = f_{c1} - \nu_{cxy} \tan(90 - \theta_\sigma) \quad (2.3.9)$$

Where f_{c1} is the principal tensile stress in the concrete.

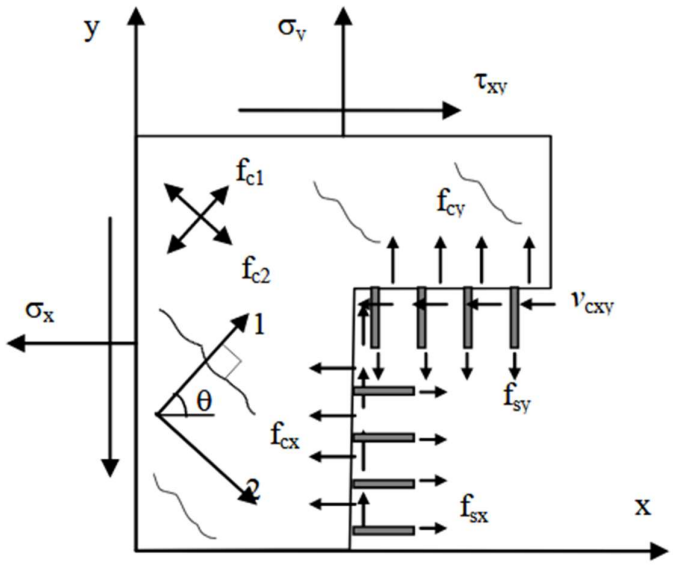

Figure 13 Average stresses in reinforced concrete (Vecchio 2013)

Constitutive Relationships

These equations connect the stresses in the equilibrium relationships to the strains in the compatibility relationships. Mainly they focus on describing concrete in tension and compression.

For concrete in compression Vecchio and Collins (1986) observed from pure shear panel tests the decrease of compressive strength with the increase of tension strains. This compression softening effect is included in the following relationship:

$$f_{c2} = \frac{f'_c[2\left(\frac{\varepsilon_{c2}}{\varepsilon_0}\right)-\left(\frac{\varepsilon_{c2}}{\varepsilon_0}\right)^2]}{0.8-0.34\left(\frac{\varepsilon_{c1}}{\varepsilon_0}\right)}$$

(2.3.10)

Where f_{c2} = principal compressive stress; ε_{c2}= principal compressive strain; f'_c= peak compressive stress; ε_0= concrete cylinder strain corresponding to f'_c; ε_{c1}= principal tensile strain.

For concrete in tension it is necessary to determine the cracking strength, f'_t, and its corresponding strain, ε_{cr}.

$$f'_t = 0.33\sqrt{f'_c} \qquad \text{(measured in MPa)}$$

(2.3.11)

$$\varepsilon_{cr} = \frac{f'_t}{E_c}$$

(2.3.12)

$$E_c = 5000\sqrt{f'_c} \qquad \text{(measured in MPa)}$$

(2.3.13)

Where E_c is the initial Young's modulus of the concrete.

In its first stage, prior to cracking, the concrete has a linear-elastic behavior.

$$f_{c1} = E_c * \varepsilon_{c1} \qquad \text{for } 0 < \varepsilon_{c1} < \varepsilon_{cr}$$

After cracking, tension stiffening can occur, due to the bond interaction between reinforcement and concrete. This is also considered with decrease of f_{c1} with the increase of ε_{c1} as follows:

$$f_{c1} = \frac{f't}{1+\sqrt{200\varepsilon_{c1}}}$$

(2.3.14)

As regards to the reinforcement behavior, it can be described with the bilinear relationship between stresses and strains as follows:

$$f_{sx} = E_s * \varepsilon_{sx} \leq f_{sxyield}$$

(2.3.15)

$$f_{sy} = E_s * \varepsilon_{sy} \leq f_{syyield}$$

(2.3.16)

Where E_s= elastic modulus for reinforcement

$f_{sxyield}$, $f_{syyield}$= yield stresses in the x and y-directions

Modelling of concrete strengthened with FRP

First of all, in VecTor2 program FRP sheet is defined as smeared reinforcement. Thus it is evenly distributed throughout the region where it is applied. The main characteristics, which are implemented in the software are the reinforcement direction with respect to horizontal axis, fabric thickness, yield/ultimate strength, elastic modulus and strain hardening strain. Important to note that several FRP layers can be modelled by inputting several layers of smeared reinforcement in the same concrete matrix.

From the analysis point of view, the software's default concrete and reinforcement models are used except the compression pre-peak behavior of concrete, where Popovics model is used instead of Hognestad (parabola).

Modelling of concrete strengthened with UHPFRC

UHPFRC is modelled as normal concrete with defining characteristics such as Cylinder compressive strength, Tensile strength, Elastic modulus and maximum aggregate size. If the latter two are not given, default values of elastic modulus E_c=50GPa and maximum aggregate size a_g= 1mm are to be used. Also crack spacing is limited to 75% of the length of fiber used.

In terms of fiber, the important aspects are the fiber type, the fiber volume ratio, the fiber length, the fiber diameter the fiber tensile strength and the fiber bond strength. If latter not given, an estimated value of $0.75\sqrt{(f'c)}$ is to be used.

From the analysis point of view, default models will be used except for concrete compression pre/post peak where Lee et al 2011 (FRC) will be used, tension softening where Exponential mode is adopted and FRC tension where DEM (Lee et al 2011) mode is selected.

3. Modelling of deep beams strengthened with FRP sheets

3.1. Experimental data

In order to study the behavior of deep beams strengthened with FRP sheets, several articles concerning the topic were reviewed and test data were collected. One major criteria was to find experimental studies, which focused on deep beams that is beams with shear-span-to-depth ratios a/d smaller or equal to 2. This way a proper shear failure could develop in the samples prior to flexural failure. Another criteria was to find tests, which had samples large enough for the size of them not the affect the outcome of the results.

Two experimental studies were selected, namely Rasheed (2016) and Bukhari et al. (2013).

The properties of the test specimens are summarized in Table 3 and geometrical properties are presented in Figure 14.

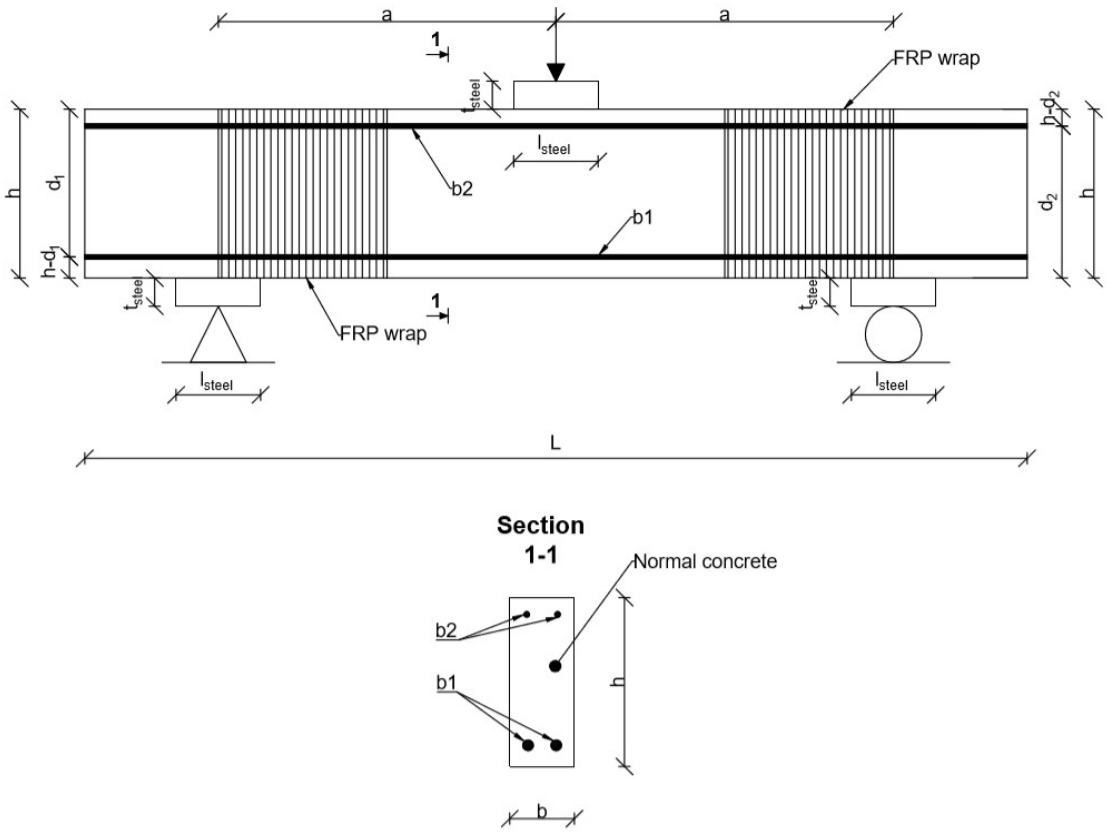

Figure 14 Test setup of beams retrofitted with UHPFRC (C-9, Bukhari et al series)

Author	Year	Beam name	L [mm]	b [mm]	h [mm]	d_1 [mm]	d_2 [mm]	a [mm]	a/d [-]	nr_{b1}	Φ_{b1} [mm]	nr_{b2}	Φ_{b2} [mm]	$f_{yk\,b1,b2}$ [MPa]	ρ_v [%]	ρ_h [%]	$f_{yk\,v,h}$ [MPa]
Rasheed	2016	DB1	1200	115	400	365	373	400	1.10	2	20	2	4	500	0	0	400
		DB2	1200	115	400	365	373	400	1.10	2	20	2	4	500	0.25		400
		DB3	1200	115	400	365	373	400	1.10	2	20	2	4	500	0.52		400
		DB4	1200	115	400	365	373	400	1.10	2	20	2	4	500	0.3	0	400
		DB5	1200	115	400	365	373	400	1.10	2	20	2	4	500	0.5	0	400
		DB6	1200	115	400	365	373	400	1.10	2	20	2	4	500	0	0.3	400
		DB7	1200	115	400	365	373	400	1.10	2	20	2	4	500	0	0.5	400
		DB8	1200	115	500	465	473	400	0.86	2	20	2	4	500	0.25		400
		DB9	1200	115	333	298	306	400	1.34	2	20	2	4	500	0.25		400
Bukhari et al	2013	C-1	1675	150	300	262.5	270	525	2	2	19	2	10	494	-	-	-
		C-2	1675	150	300	262.5	270	525	2	2	19	2	10	494	-	-	-
		C-3	1675	150	300	262.5	270	525	2	2	19	2	10	494	-	-	-
		C-4	1675	150	300	262.5	270	525	2	2	19	2	10	494	-	-	-
		C-5	1675	150	300	262.5	270	525	2	2	19	2	10	494	-	-	-
		C-6	1675	150	300	262.5	270	525	2	2	19	2	10	494	-	-	-
		C-7	1675	150	300	262.5	270	525	2	2	19	2	10	494	-	-	-
		C-8	1675	150	300	262.5	270	525	2	2	19	2	10	494	-	-	-
		C-9	1675	150	300	262.5	270	525	2	2	19	2	10	494	-	-	-
		C-10	1675	150	300	262.5	270	525	2	2	19	2	10	494	-	-	-
		C-11	1675	150	300	262.5	270	525	2	2	19	2	10	494	-	-	-
		C-12	1675	150	300	262.5	270	525	2	2	19	2	10	494	-	-	-

L= total length of the beam; b= width of the beam; h= height of the beam; d_1,d_2= effective depths of the sections with respect to bottom and top longitudinal reinforcment; a= shear-span; a/d= span-to-depth ratio; nr_{b1},nr_{b2} = no. of bottom and top longitudinal bars; Φ_{b1}, Φ_{b2}= diameter of bottom and top longitudinal bars; $f_{yk\,b1,b2}$= yield strength of longitudinal bars; ρ_v,ρ_h= vertical and horizontal shear reinfocement ratio; $f_{yk\,v,h}$ = yield strength of shear reinforcement

Table 3 Gathered data

Author	Year	Beam name	f'_c [MPa]	a_g [mm]	Steel plates			FRP sheets				Epoxy resin		
					t_{steel} [mm]	b_{steel} [mm]	l_{steel} [mm]	t [mm]	f_{yf} [MPa]	E_f [GPa]	esh [%]	f_{yep} [MPa]	E_{ep} [Gpa]	t_{opt} [mm]
Rasheed	2016	DB1	34	10	20	115	75/150	0.13	3500	230	1.5	30	3.8	1
		DB2	34	10	20	115	75/150	0.13	3500	230	1.5	30	3.8	1
		DB3	34	10	20	115	75/150	0.13	3500	230	1.5	30	3.8	1
		DB4	34	10	20	115	75/150	0.13	3500	230	1.5	30	3.8	1
		DB5	34	10	20	115	75/150	0.13	3500	230	1.5	30	3.8	1
		DB6	34	10	20	115	75/150	0.13	3500	230	1.5	30	3.8	1
		DB7	34	10	20	115	75/150	0.13	3500	230	1.5	30	3.8	1
		DB8	34	10	20	115	75/150	0.13	3500	230	1.5	30	3.8	1
		DB9	34	10	20	115	75/150	0.13	3500	230	1.5	30	3.8	1
Bukhari et al	2013	C-1	49.13	19	50	150	150	-	-	-	-	-	-	-
		C-2	49.1	19	50	150	150	0.34	3450	234.5	-	-	-	-
		C-3	48.28	19	50	150	150	0.34	3450	234.5	-	-	-	-
		C-4	49.1	19	50	150	150	0.34	3450	234.5	-	-	-	-
		C-5	48.62	19	50	150	150	0.34	3450	234.5	-	-	-	-
		C-6	49.79	19	50	150	150	0.34	3450	234.5	-	-	-	-
		C-7	48.97	19	50	150	150	0.34	3450	234.5	-	-	-	-
		C-8	47.93	19	50	150	150	0.34	3450	234.5	-	-	-	-
		C-9	50.35	19	50	150	150	0.34	3450	234.5	-	-	-	-
		C-10	51.38	19	50	150	150	0.34	3450	234.5	-	-	-	-
		C-11	49.38	19	50	150	150	0.34	3450	234.5	-	-	-	-
		C-12	48.41	19	50	150	150	0.34	3450	234.5	-	-	-	-

f'_c= normal concrete cylinder strength; a_g= maximum aggregate size; t_{steel}= thickness of steel plates; b_{steel}=witdh of steel plates; l_{steel}= length of steel plates; t= thickness of FRP sheet; f_{yf} = yield tensile strength of FRP sheet, E_f= Young's modulus of FRP sheet; esh= ultimate strain of FRP; f_{yep}= yield tensile strength of epoxy resin; E_{ep}= Young's modulus of epoxy resin; t_{opt}= optimal thickness of epoxy application

Table 3. Gathered data (continuation)

Tests by Bukhari et al. (2013)

In this experimental program the main focus was on the behavior of different CFRP configurations applied to short beams, which were designed to fail in shear. For this cause the beams were reinforced only with longitudinal bars, adding no shear reinforcement. The same type of CFRP sheets were used for all the test specimens. The beams were arranged in two groups, namely A and B where group A had CFRP sheets over the whole height of the beam, while group B was covered only half of the height, as seen in Figure 14. Each beam was tested under a symmetrical three-point loading and the deflection was measured at mid-span and at supports. As it can be seen in Figure 14, in some cases only the position of the CFRP sheet was changed, but not the overall dimension.

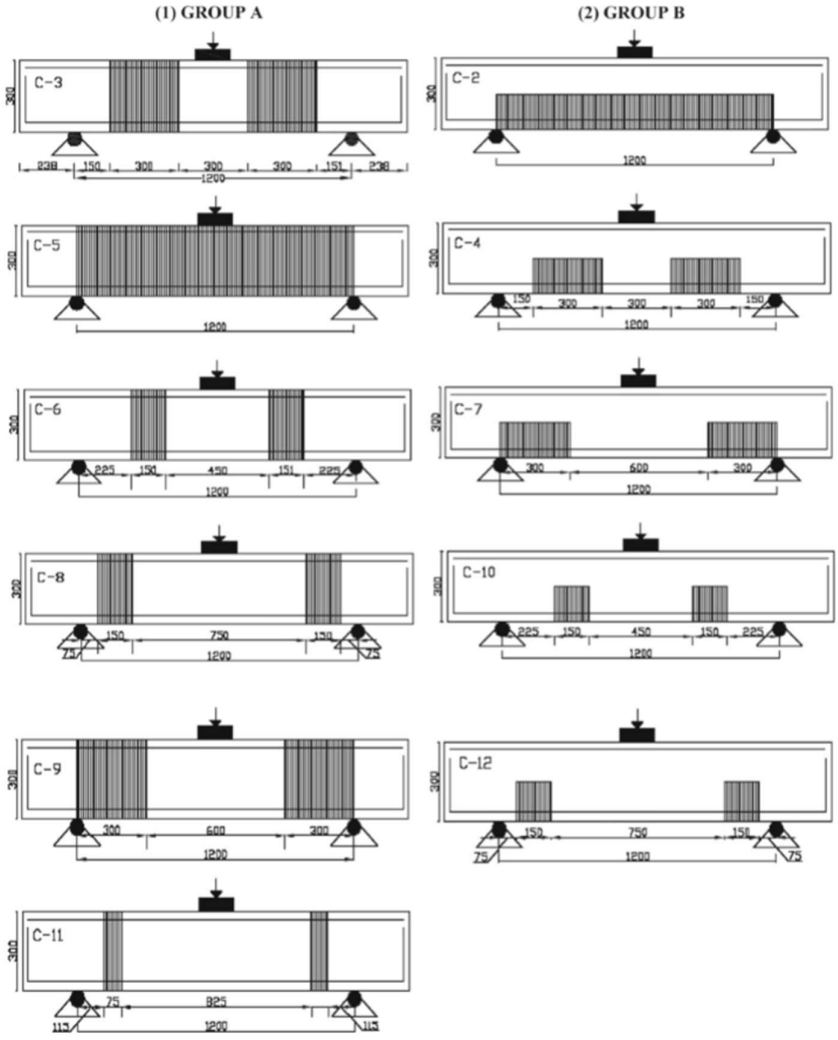

Figure 15 Beam configuration details (Bukhari et al. 2013)

Tests by Rasheed (2016)

The following experimental program was performed to investigate effect of CFRP sheets on the shear strength of reinforced concrete deep beams. The parameters studied were the shear-span-to-depth ratio a/d and the quantity of vertical and horizontal shear reinforcement in the beams. Table 4 presents the depth, a/d ratio and the shear reinforcement percentage for each beam.

Beam name	d_1 [mm]	a [mm]	a/d [-]	ρ_v [%]	ρ_h [%]
DB1	365	400	1.10	0	0
DB2	365	400	1.10	0.25	
DB3	365	400	1.10	0.52	
DB4	365	400	1.10	0.3	0
DB5	365	400	1.10	0.5	0
DB6	365	400	1.10	0	0.3
DB7	365	400	1.10	0	0.5
DB8	465	400	0.86	0.25	
DB9	298	400	1.34	0.25	

Table 4 Details of tested beams

Every beam was reinforced with the same amount of bottom longitudinal reinforcement. All beams were retrofitted with the same configuration of CFRP sheets, as seen in figure 15.

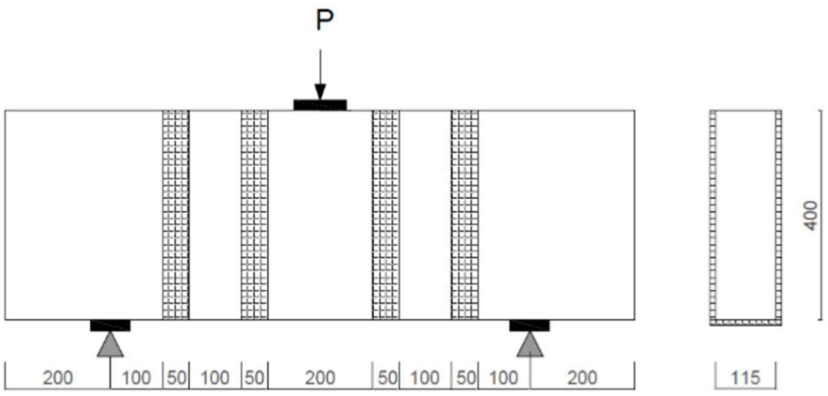

Figure 16 Configuration of CFRP sheets on the reinforced deep beams (Rasheed, 2016)

This experiment was also performed a under three-point loading scheme. The load and support reactions were introduced via steel plates to avoid local concrete crushing. Mid-span deflections were measured with a dial gauge.

Firstly, all deep beams were tested until failure. Then CFRP retrofitting was applied to them. Lastly the retrofitted beams were loaded until failure.

3.2. Finite element models of test specimens

Tests by Bukhari et al. (2013)

Figure 17 shows the finite element model (FEM) of beam C-3 built in program VecTor2. As one can see, the beam is defined as a simply supported one, having a pin support on the left side and a roller on the right. The load was applied as displacements uniformly distributed on the top steel plate in order to capture the post-peak behavior of the beam. Steel plates (material C) were placed in both support and load points.

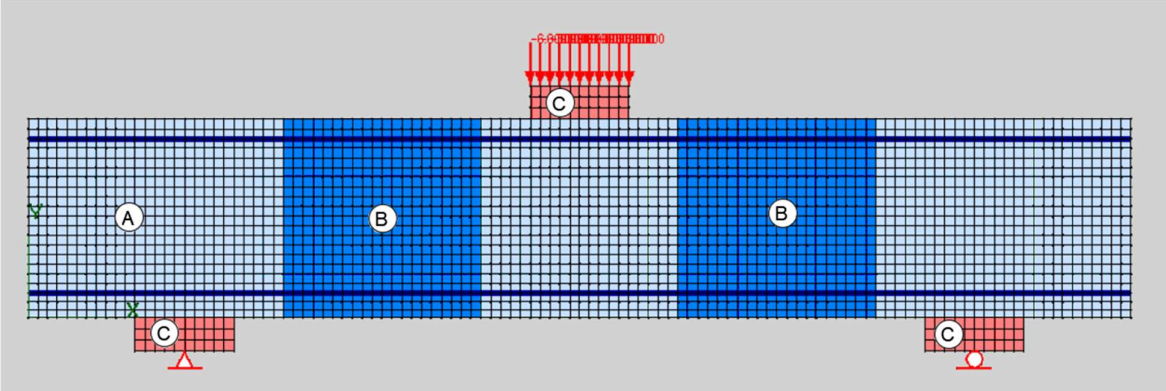

Figure 17 Finite element model of Bukhari et al. test series (model C-3)

The FEM consists of two types of finite elements: quadrilateral elements, used for the modelling of concrete and steel plates, and truss elements used for the longitudinal reinforcement. A perfect bond is defined between the longitudinal reinforcement and the surrounding concrete, as well as between the concrete and retrofitting material. The mesh size used in the model for the quadrilateral elements is of 15x15 mm, to avoid unrealistically stiff behavior.

Because the FE program works in a 2D, with principal axes X and Y, the thickness of the element is given as property. This is the same for each material type, and has the value of 150mm.

Material A represents the normal concrete. Its main characteristics are the cylinder compressive strength f'_c=49.1 MPa and the maximum aggregate size a_g= 19mm.

Material B represents the concrete part of the beam, which was retrofitted with the CFRP sheets. It has the same concrete properties as material A, with the addition of CFRP as smeared reinforcement. This CFRP layer is characterized by its thickness t=0.34 mm, tensile strength f_{yf}= 3450 MPa and Young's modulus E_f=234.5 GPa.

Material C are the aforementioned steel plates, having a yield strength f_y= 500 MPa.

Tests by Rasheed (2016)

In Figure 18 the finite element model of beam RDB1 built in program Vector2 is presented. In order to reduce compilation time of models, the experimental specimens were modelled as half-beams. One roller was positioned at the end of the beam, while several others were installed in the middle of the beam in order to represent continuity of the beam. Thus the whole system acts like a simply supported beam.

Displacements were uniformly distributed on the loading plate at the top of the beam in order to capture the post-peak behavior of the beam. Steel plates (Material D) were placed under load and over support to prevent concrete crushing.

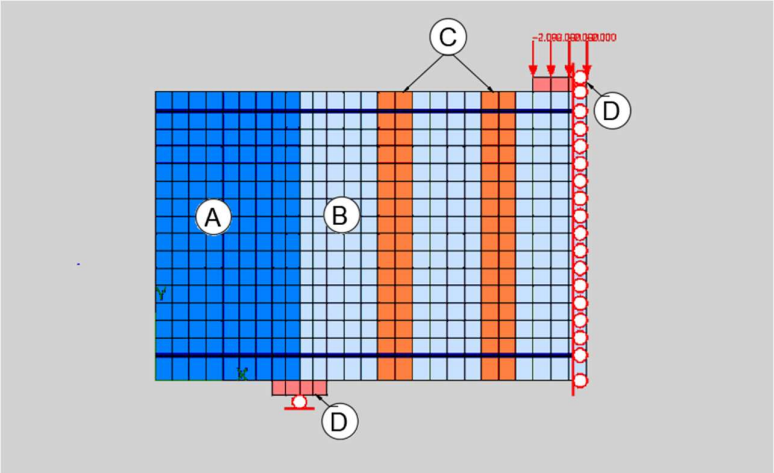

Figure 18 Finite element model of Rasheed test series (Model RDB1)

The FEM consists of two types of finite elements: quadrilateral elements, used for the modelling of concrete and steel plates, and truss elements used for the longitudinal reinforcement. A perfect bond is defined between the longitudinal reinforcement and the surrounding concrete, as well as between the concrete and retrofitting material.

To achieve better results, different mash sizes were used. In vertical plane of the support region a mesh size of 20x25 mm was applied, whilst in other regions a square mesh of 25x25 mm was used. The different mesh near the support helps to define the roller at the center, thus no alteration from the original test is made.

Material A represents the normal concrete with existing web reinforcement. Besides the horizontal and vertical shear reinforcements, which vary from beam to beam, an extra amount of vertical stirrups (Φ4/ 50mm) were added to tie together the longitudinal bars. Otherwise it has the same properties as Material B.

Material B represents the normal concrete. It has a cylinder compressive strength of f'_c=34 MPa, and its maximum aggregate size is a_g =10 mm.

Material C represents the concrete part of the beam, which was retrofitted with the CFRP sheets. It has the same concrete properties as material B, with the addition of CFRP as smeared reinforcement. This CFRP layer is characterized by its thickness t=0.13 mm, tensile strength f_{yf}= 3500 MPa, Young's modulus E_f=234.5 GPa and a maximum elongation of 1.5%.

Material D represents the steel plates, having a yield strength f_y= 500 MPa.

3.3. Discussion of results

Tests by Bukhari et al. (2013)

The test specimens from the two distinct groups shown in Figure 15 showed different behavior which was captured with different accuracy by the finite element models. Group A, where the FRP sheets was applied on the whole height of the beam, showed better agreement between experiment and prediction results. For example, beam C-3, which is represented in Figure 17, had an experimental failure load of 307 kN, while the predicted value is 300 kN. This represents an error of 3%. For further discussion of Group A, beam C-3 will be used as example.

In Figure 19 the crack patterns of FEM and experiment are presented and analyzed. For FEM the thin red lines represent the cracks in the finite elements, where the line thickness is indicative of the crack width. In FEM the FRP sheets prevented shear cracks and made the reinforcement yield, thus flexural failure was achieved. In case of experiment though flexural and shear cracks appeared at the same time, due to the cause of delamination of FRP sheets. Still the behavior of the prediction and experiment were in good accordance.

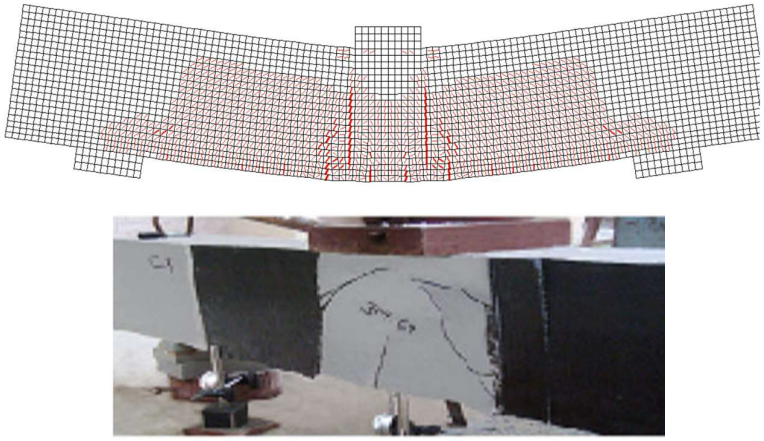

Figure 19 Comparison of crack patterns at failure load between FE model and experiment (beam C-3)

Figure 20 shows the measured and predicted response of beam C-3 up to failure. As it can be seen, the complete response of the beam is very well captured by the FEM. The stiffness of FEM is in compliance with the experimental result. The yield plateau due to yielding of bottom longitudinal reinforcement is also well captured. The above mentioned observations are valid for all specimens from group A. This is confirmed by the low average error value of only 3.8%.

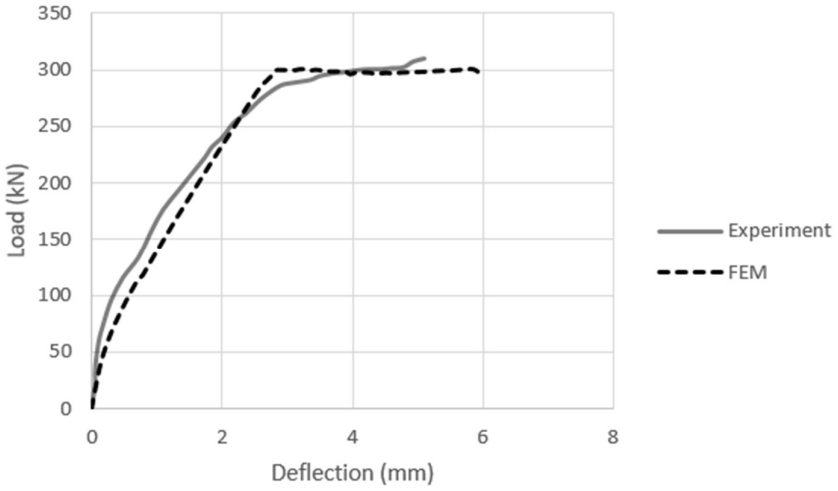

Figure 20 Load-deflection curve of deep beam C-3

On the other hand, the specimens from Group B, where FRP sheets were applied only on half of the beam height, results showed poor agreement between experiment and predictions. For further discussion beam C-4 is used as example.

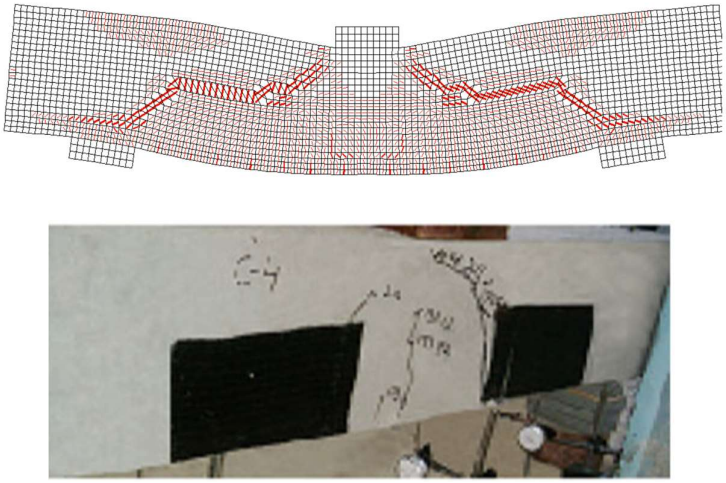

Figure 21 Comparison of crack patterns at failure load between FE model and experiment (beam C-4)

First of all, one has to examine the crack patterns of FEM and experiment seen in Figure 21. As it can be noticed, in case of FEM the cracks, not being able to pass through the FRP region with higher stiffness and perfect bond between concrete and FRP, take the rout above the FRP sheet. Due to this cause the FEM specimens tend to underperform. In case of experiment this phenomenon does not happen due to early debonding of FRP sheets. Thus the cracks propagate as anticipated by the strut-and-tie-model for deep beams.

As seen in Figure 22, the load-deflection curve of FEM and experiment also differ. In the first portion of the curve the FEM shows good agreement with the experiment. Near the 200 kN

load a sudden drop occurs in FEM. This is the moment, when critical cracks above FRP sheets appear. In the end portion of the curve the FEM value gets closer to the experimental one again.

Similar behavior of cracks were observed at beams C-7 and C-10 also. These samples had an average error of 20%, the highest one recorded at C-10, having the value of 32%. In every case the FEM underestimated the performance of the specimens.

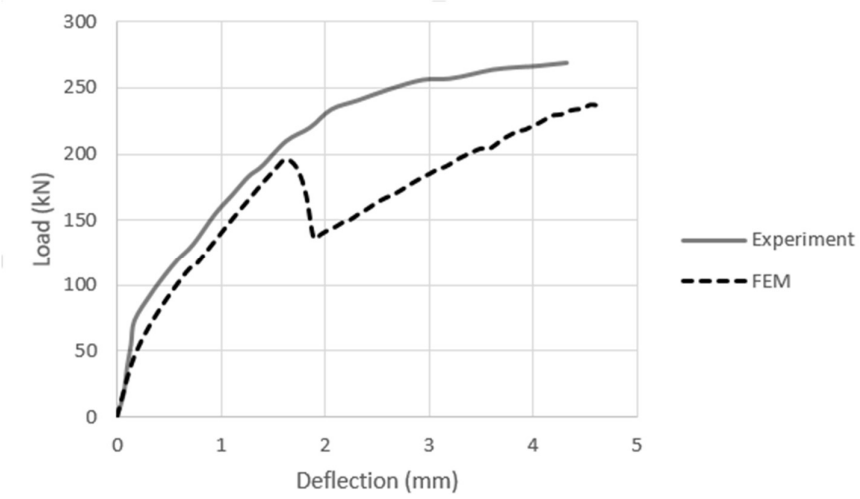

Figure 22 Load-deflection curve of deep beam C-4

Figure 23 summarizes the experimental and predicted values of failure loads for each beam. As it can be seen, applying FRP sheet only at the half of the beams have a small or even no effects on the shear strength of the element. In this case it can be more beneficial to place FRP sheets close to the support for greater effect. As expected, with the increase of areas covered with FRP sheets, the failure load also increases. In group B a gradual increase of capacity is seen, up to 27% in case of experimental data and up to 13% from predictions. This difference is caused by the overestimation of failure load at the unretrofitted beam C-1 and underestimation at C-2.

In group A a similar increase can be noticed with a larger slope, capacity increase from control beam to fully wrapped retrofitted beam (C-5) being as high as 55% in case of experimental data and 41% from predictions. Here also beams with FRP placed near supports, such as C-8, or C-9, show similar or better results, than beams with same amount of FRP used, but placed in different configuration (C-3, C-6).

In general use of FRP sheets caused the increase of shear strength and stopped crack propagation. It also caused the retrofitted beams to fail in flexure rather than shear.

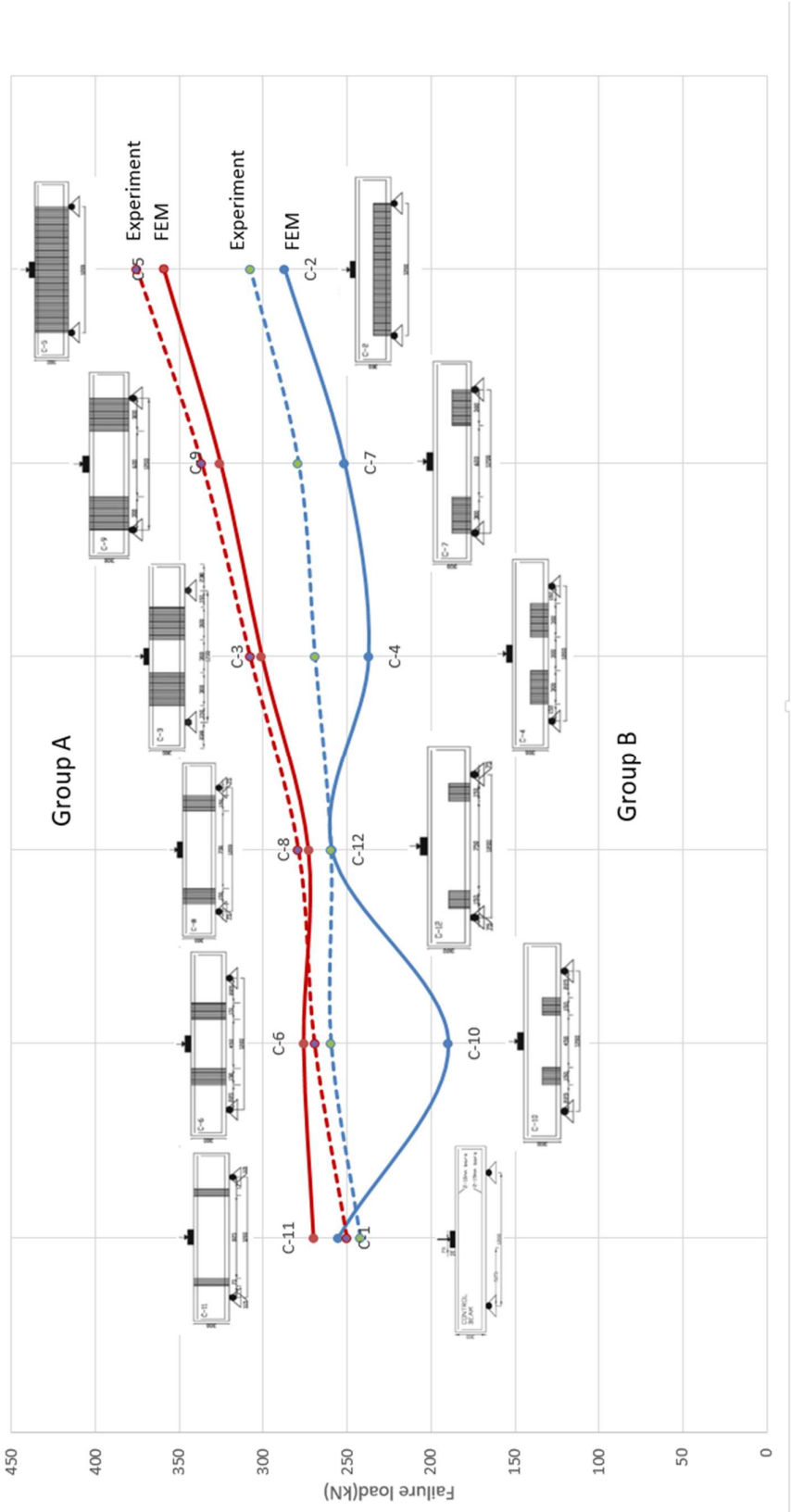

Figure 23 Comparison between experimental and predicted values of beam failure loads

Tests by Rasheed (2016)

As mentioned earlier this experimental program featured two main variables, namely the shear reinforcement ratio and the shear-span-to-depth ratio of the deep beams.

Firstly the effects of shear reinforcement will be discussed. In total seven beams were analyzed. RDB1 has no shear reinforcement, RDB2 and RDB3 have both vertical and horizontal shear reinforcement, RDB4 and RDB5 have only vertical shear reinforcement, while RDB6 and RDB7 were reinforced with horizontal shear reinforcement. For further discussion, beam RDB3 will be used as example.

In Figure 24 the load deflection curve of RDB3 is presented. As it can be seen, even if the stiffness is well predicted, the FEM overestimates the experimental failure load. This is caused by debonding during the experiment, which cannot be modelled in VecTor2.

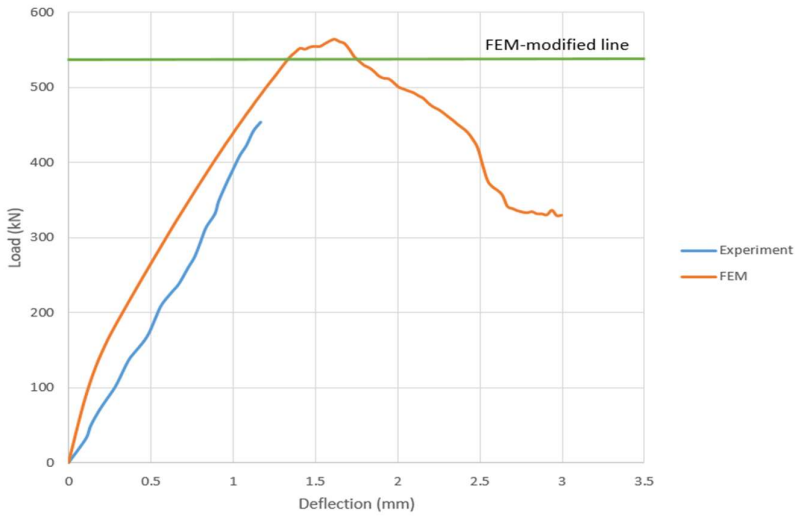

Figure 24 Load-deflection curve of RDB3

In order get better estimation of results, American design code ACI 440.2R-08 is used to calculate the vertical strains at which debonding occurs. Then the analysis is stopped at the respective limit, and the beam is considered failed at FEM-modified line. In order to better understand the background of the design code, we need to analyze what parameters does it use. ACI 440.2R-08 design code takes into consideration the active bond length of FRP sheets rather then the whole wrap, the thickness of FRP sheets and the strength of the concrete, as seen in the following equations

$$\varepsilon_{fe} = K_v * \varepsilon_{fu} \leq 0.004 \qquad (1)$$

$$K_v = \frac{k_1 * k_2 * L_e}{11900 * \varepsilon_{fu}} \qquad (2)$$

$$L_e = \frac{23300}{(n_f t_f E_f)^{0.58}} \qquad (3)$$

$$k_1 = \left(\frac{f'_c}{27}\right)^{2/3} \qquad (4)$$

$$k_2 = \frac{d_{fv} - 2*L_e}{d_{fv}} \qquad (5)$$

Where: ε_{fe}= effective strain in FRP laminates; K_v= bond reduction coefficient; L_e= active bond length; n_f= modular ratio of elasticity between FRP and concrete; t_f= nominal thickness of FRP reinforcement; E_f= tensile modulus of elasticity of FRP; k_1,k_2= modification factors; f'_c= specified compressive strength of concrete; d_{fv}= effective depth of FRP shear reinforcement.

Figure 25 summarizez the failure loads for the seven deep beams with different shear reinforcement ratio. The FEM-modified curve represent the values obtained from calculations made according to ACI 440.2R-08 design code.

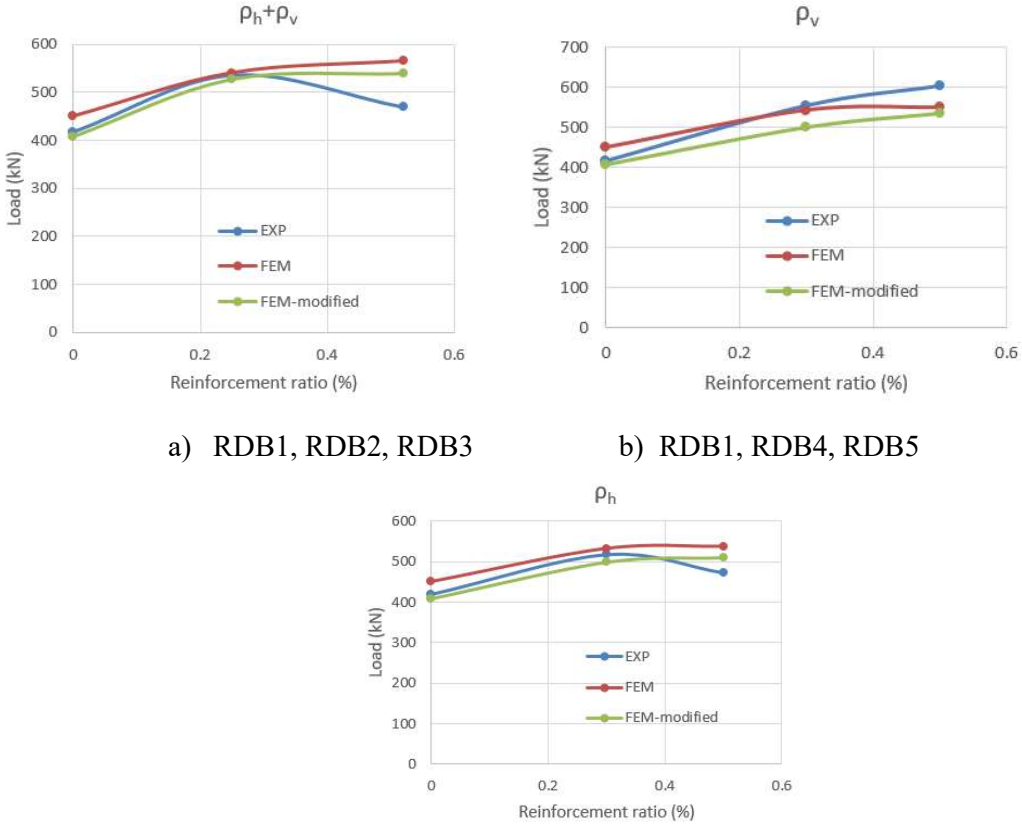

a) RDB1, RDB2, RDB3 b) RDB1, RDB4, RDB5

c) RDB1, RDB6, RDB7

Figure 25 FEM failure loads for Rasheed series

Even though the FEM- modified curve does not improve the average error, which is 7% throughout the seven beams, it helps in reducing the maximum deflection of results from 17% to 13%. Indeed it can be challenging to determine the tensile strain of the FRP sheets at which they debond.

The issues met were present at RDB3, RDB7 and RDB5. In the first two cases early debonding was met during the experiments conducted by Rasheed, even though RDB3 and RDB7 had more shear reinforcement than RDB2 and RDB6 respectively. This can be caused by the difficult application of FRP sheets, many times bond strength differing from case to case. In case of RDB5 the experiment value was about 9% higher than the one presented in FEM. This underestimation can be caused by the localization of cracks near FRP sheets. Even though differences were met between experimental values and the ones given by FEM for failure loads, in almost every case the load-deflection curve reflected reality.

The FEM investigation also concluded the benefic impact of FRP sheets on shear strength. In case of all samples a rise in ultimate bearing load was observed, ranging from 5% strength increase up to 30% compared to un-retrofitted beams in case of predictions and from 7% to 120% in case of experimental study .

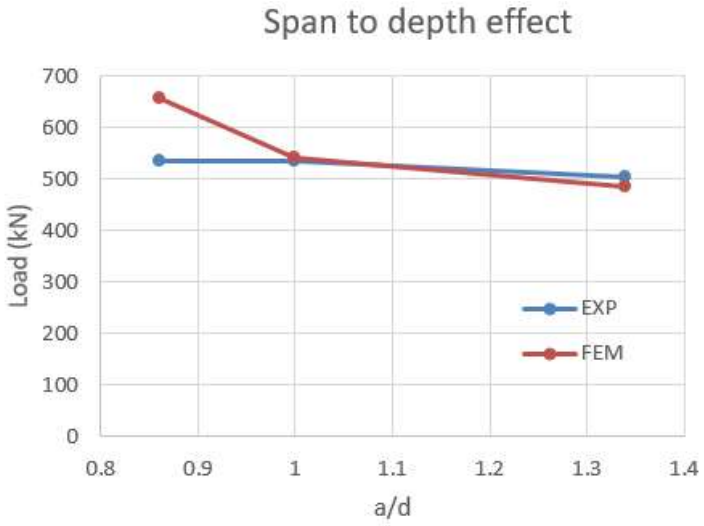

Figure 26 Failure loads at different span-to-depth ratios

Figure 28 presents the second parameter studied, namely the shear-span-to-depth ratio. For this part three beams, namely RDB2, RDB8 and RDB9 are analyzed. Every one of them has the same shear reinforcement ratio, its value being 0.25% both in horizontal and vertical directions. The different span-to-depth ratios are 0.86 for RDB8, 1 for RDB2 and 1.34 for RDB9.

It can be noticed, that as the depth of the beam decreases, so does the failure load. Indeed for deep beams with very small span-to-depth ratios the stiffness curve and the failure loads are hard to predict.

Also it can be seen, that for very deep beams, with small shear-span-to-depth ratios the differences between FEM and experiment become greater. In case of RDB8 the error is almost 19%, while in case of RDB2 and RDB9 FEM shows good agreement with experimental results, errors being 1% and 4%.

4. Modelling of deep beams strengthened with UHPFRC

4.1. Experimental data

In order to gather data from experimental studies, the same criterias were set for UHPFRC retrofitted beams as for FRP ones. Only test specimens with shear-span-to-depth ratios a/d less or equal to 2.5 were selected. Also simplicity of experiments was a key factor, in order to implement it into the finite element software. Two experimental studies were selected, namely Meda et al. (2014) and Martinola et al (2010).

The properties of the test specimens are summarized in Table 5. Due to the fact that some material characteristics were not specified in the studies, these were estimated. All the estimated values are highlighted in green. The meaning of the geometrical properties in Table 5 is illustrated in Figure 28, which depicts a typical test of an UHPFRC-strengthened beam (Meda et al. 2014).

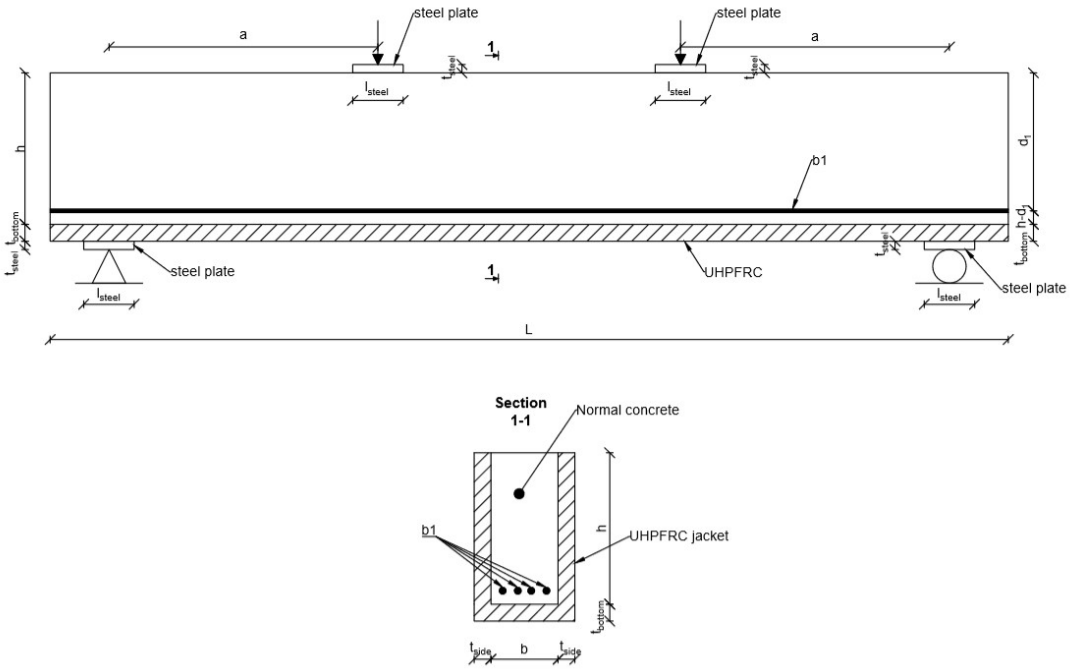

Figure 27 Test setup of beams retrofitted with UHPFRC (Beam SB, Meda et al. series)

Table 5. Gathered data for UHPFRC

Author	Year	Beam name	L [mm]	b [mm]	h [mm]	d_1 [mm]	d_2 [mm]	a [mm]	a/d [-]	nr_{b1}	Φ_{b1} [mm]	nr_{b2}	Φ_{b2} [mm]	$f_{yk\ b1,b2}$ [MPa]	ρ_v [%]	$f_{yk\ v}$ [MPa]
Meda et al	2014	Beam SR	2850	200	450	410	-	800	1.95	4	20	-	-	518	-	-
		Beam SA	2850	200	450	410	-	800	1.95	4	20	-	-	518	-	-
		Beam SB	2850	200	450	410	-	800	1.95	4	20	-	-	518	-	-
		Beam SC	2850	200	450	410	-	800	1.95	4	20	-	-	518	-	-
		Beam SD	2850	200	450	410	-	800	1.95	4	20	-	-	518	-	-
Martinola et al	2010	NCB	4550	300	500	455	460	1090	2.40	2	16	2	12	560	0.23	560
		UHPCB-no steel	4550	300	500	455	460	1090	2.40	-	-	-	-	-	-	-
		UHPCB-with steel	4550	300	500	455	460	1090	2.40	2	16	2	12	560	0.23	560

L= total length of the beam; b= width of the beam; h= height of the beam; d_1,d_2= effective depths of the sections with respect to bottom and top longitudinal reinforcment; a= shear span; a/d= span-to-depth ratio; nr_{b1},nr_{b2} = no. of bottom and top longitudinal bars; Φ_{b1}, Φ_{b2}= diameter of bottom and top longitudinal bars; $f_{yk\ b1,\ b2}$= yield strength of longitudinal bars; ρ_v= vertical shear reinfocement ratio; $f_{yk\ v}$ = yield strength of shear reinforcement

				Steel plates			UHPFRC									Fibers				
Author	Year	Beam name	f'_c [MPa]	t_{steel} [mm]	b_{steel} [mm]	l_{steel} [mm]	t_{bottom} [mm]	$f'_{c,bot}$ [MPa]	$a_{g,bot,side}$ [mm]	$f_{ct,bot}$ [MPa]	E_{bot} [GPa]	t_{side} [mm]	$f'_{c,\ side}$ [MPa]	$f_{ct,side}$ [MPa]	E_{side} [GPa]	Type	V_f [%]	L_f [mm]	Φ_f [mm]	f_{uf} [MPa]
Meda et al	2014	Beam SR	32.6	25	200	150	-	-	-	-	-	-	-	-	-	-	-	-	-	-
		Beam SA	32.6	25	200	150	30	108	1	6.66	38	30	108	6.66	38	Straight	1.25	15	0.175	2000
		Beam SB	32.6	25	200	150	50	108	1	6.66	38	50	108	6.66	38	Straight	1.25	15	0.175	2000
		Beam SC	32.6	25	200	150	50	108	1	6.66	38	50	75	4.68	33	Straight	1.25	15	0.175	2000
		Beam SD	32.6	25	200	150	50	108	1	6.66	38	30	75	4.68	33	Straight	1.25	15	0.175	2000
Martinola et al	2010	NCB	22	20	300	80	-	-	-	-	-	-	-	-	-	-	-	-	-	-
		UHPCB-no steel	22	20	300	80	40	177	1.3	-	50	40	177	-	50	Straight	2.5	12	0.18	2850
		UHPCB-with steel	22	20	300	80	40	177	1.3	-	50	40	177	-	50	Straight	2.5	12	0.18	2850

f'c= normal concrete cylinder strength; t_{steel}= thickness of steel plates; b_{steel}=witdh of steel plates; l_{steel}= length of steel plates; t_{bottom}= thickness of UHPFRC bottom layer; $f'_{c,bot}$= cylinder strength of UHPFRC bottom layer; $a_{g,\ bot,\ side}$= maximum size of aggregates in UHPFRC bottom and side layers; $f_{ct,bot}$= tensile strength of UHPFRC bottom layer; E_{bot}=Young's modulus in UHPFRP bottom layer; t_{side}= thickness of UHPFRC side layer; $f'_{c,side}$= cylinder strength of UHPFRC side layer; $f_{ct,side}$= tensile strength of UHPFRC side layer; E_{side}=Young's modulus in UHPFRP side layer; V_f= fiber volume ratio; L_f= fiber length; Φ_f= fiber diameter; f_{uf}= fiber ultimate tensile strength

Tests by Meda et al. (2014)

The focus of the test program by Meda et al. (2014) was on the behavior of short beams retrofitted with U-shape UHPFRC jackets. The original beams were designed to have shear failure. For this purpose only longitudinal reinforcement was used in the bottom part of the beams to resist bending. The parameters studied were the type of UHPFRC and the thickness of the jackets. Two types of UHPFRC mixes were used, namely a self-leveling concrete and a thixotropic concrete. Self-leveling concrete jacket was applied by casting in molds, whilst thixotropic concrete was directly applied to the surfaces of the beams. Prior to UHPFRC application the surface of the beams were sandblasted in order to obtain perfect bond between normal concrete and retrofit material. The thicknesses of the jackets were ranging from 30 to 50 mm. One beam was used as a control specimen, while four other beams were retrofitted in different configurations as follows:

- Beam SA had 30mm-thick self-levelling concrete applied to its bottom and side faces
- Beam SB had 50mm-thick self-levelling concrete applied to its bottom and side faces
- Beam SC had 50mm-thick self-levelling concrete applied to its bottom face and 50 mm thick thixotropic concrete on the side faces
- Beam SD had 50mm-thick self-levelling concrete applied to its bottom face and 30 mm thick thixotropic concrete on the side faces

All beams were tested in four-point bending as shown in Figure 28. It can be seen that the load and support reactions were introduced via steel plates in order to avoid local concrete crushing. The test measurements included the applied load and the mid-span deflection.

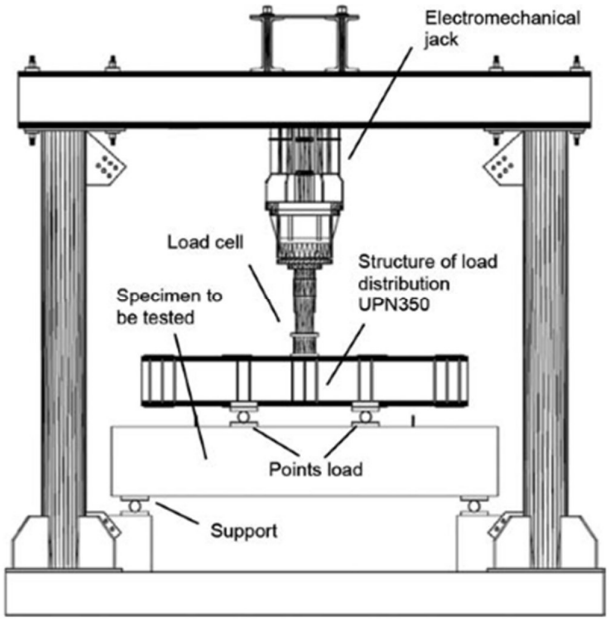

Figure 28 Loading frame (Meda et al. 2014)

Tests by Martinola et al. (2010)

The following experimental program was performed to investigate the effect of UHPFRC strengthening on full scale reinforced concrete beams. Figure 29 shows the geometry of the specimens and the strengthening scheme. A total number of three beams were tested for this experiment. One beam was cast without any reinforcement, while other two were reinforced with longitudinal and shear reinforcement as seen in Figure 29.

One beam with reinforcement was used as reference, while the other two were retrofitted with 40mm thick UHPFRC layers on bottom and side faces. In order to create an adequate bond strength between reinforced concrete and strengthening material, the beams were sandblasted prior to application of UHPFRC jackets. The jackets were applied directly to the beams, without vibration. Curing of test specimens was carried out at ambient temperature and humidity.

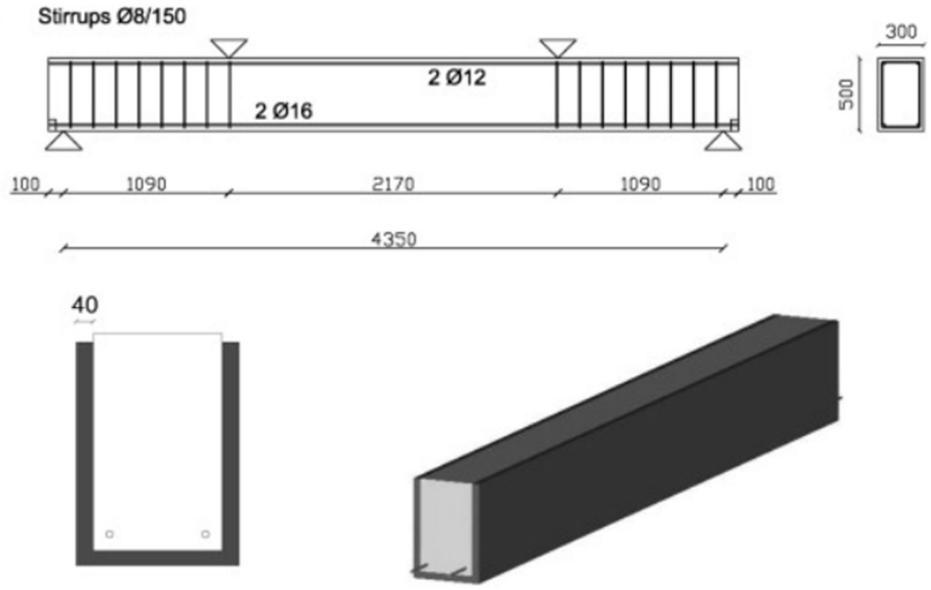

Figure 29 Geometry of specimens and strengthening scheme (Martinola et al. 2010)

All beams were tested in four-point bending. Load and support reactions were introduced via steel plates in order to avoid local concrete crushing. The test measurements included the applied load and the mid-span deflection.

4.2. Finite element models of test specimens

Tests by Meda et al. (2014)

Figure 30 shows the finite element model of beam Beam SC built in program VecTor2. As one can see, the model is represents a simply supported beam, with a pin support on the left side and a roller on the right. Two displacements of 35 mm each were applied on the loading plates at the top of the beam in order to capture the post-peak behavior of the beams. Steel plates (material C) were placed in both support and load points.

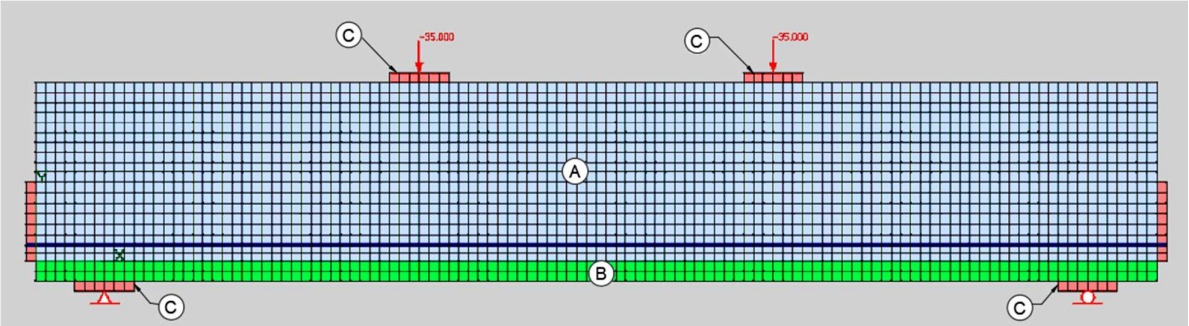

Figure 30 Finite element model of Meda et al. test series (model Beam SC)

The FEM consists of two types of finite elements: quadrilateral elements, used for the modelling of concrete and steel plates, and truss elements used for the longitudinal reinforcement. A perfect bond is defined between the longitudinal reinforcement and the surrounding concrete, as well as between the concrete and retrofitting material. The mesh size used in the model for quadrilateral elements is of 25x25 mm.

Material A represents the normal concrete. Its main characteristic is the cylinder compressive strength f'_c=32.6 MPa. No shear reinforcement is used.

Material B represents the UHPFRC. It has a cylinder compressive strength f'_c=108 MPa, tensile strength f'_t=6.66 MPa, Young's Modulus E_f=38 GPa and a maximum aggregate size $a_{g,bot}$= 1mm. It contains straight steel fibers with fiber volume ratio V_f= 1.25%, fiber length l_f=15 mm, fiber diameter Φ_f=0.175 mm, fiber tensile strength F_u= 2000 MPa, and fiber bond strength T_u=7.8 MPa.

Material C represents the steel plates, having a yield strength f_y= 500 MPa.

Because program VecTor2 works in 2D, other two regions were defined parallel to the region of Material A. These two regions represent the side UHPFRC layers and have the following characteristics: f'_c=75 MPa, tensile strength f'_t=4.68 MPa, Young's Modulus E_f=33 GPa and maximum aggregate size $a_{g,side}$= 1mm. They have the same fiber properties as Material B.

Tests by Martinola et al. (2010)

In Figure 31 one can see the finite element model of beam UHPCB built in program VecTor2. The experimental specimens were modelled as half-beams, thus compilation time was greatly reduced. One roller was positioned at the end of the beam, while several others were installed in the place where the middle of the beam is in reality. Thus the whole system acts like a simple supported beam, and continuity of beam in the middle is not compromised.

One displacement of 15 mm was placed on the loading plate at the top of the beam in order to capture the post-peak behavior of the beam. Steel plates were placed over the support and under the load to prevent concrete crushing.

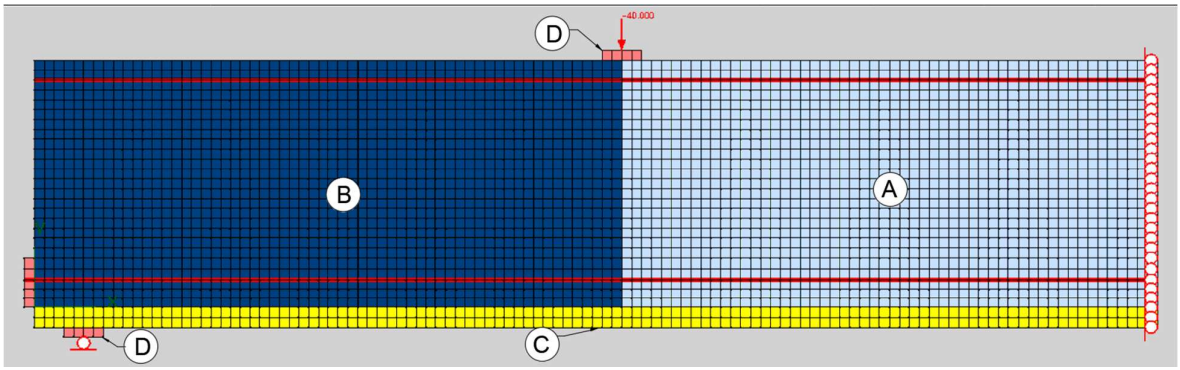

Figure 31 Finite element model of Martinola et al. test series (model UHPCB)

The FEM consists of two types of finite elements: quadrilateral elements, used for the modelling of concrete and steel plates, and truss elements used for the longitudinal reinforcement. A perfect bond is defined between the longitudinal reinforcement and the surrounding concrete, as well as between the concrete and retrofitting material. The mesh size used in the model for quadrilateral elements is of 20x20 mm.

Material A represents the normal concrete. Its main characteristic is the cylinder compressive strength f'_c=22 MPa.

Material B represents the normal concrete with stirrups. Its main characteristic is the cylinder compressive strength f'_c=22 MPa and has stirrups with diameter Φ8 positioned at distance of 150 mm.

Material C represents the UHPFRC. It has the cylinder compressive strength f'_c=177 MPa, Young's Modulus E_f=50 GPa and maximum aggregate size $a_{g,bot}$= 1.3mm. It contains straight steel fibers with fiber volume ratio V_f= 2.5%, fiber length l_f=12 mm, fiber diameter Φ_f=0.18 mm, fiber tensile strength F_u= 2850 MPa, and fiber bond strength T_u=10 MPa.

Material D represents the steel plates, having a yield strength f_y= 500 MPa.

Because program VecTor2 works in 2D, other two regions were defined parallel to the regions of Material A and B. These two regions represent the side UHPFRC layers and have the same characteristics as Material C.

4.3. Discussion of results

Tests by Meda et al. (2014)

As mentioned before, different UHPFRC layers with different thicknesses were applied on the beams tested by Meda et al. (2014). In order to highlight the behavior of an UHPFRC-strengthened beam, the results from Beam SC are discussed first in some detail.

As shown in Figure 32, the predicted crack patterns of the beam are compared to the measured pattern at failure. It can be observed that in the FEM the critical crack is located in the middle of the beam, while in the in the experiment it was located near the left load point. This can happen due to material imperfections or localization of stresses in the reinforcement. Nevertheless several similarities can also be noticed, such as the multiple vertical cracks between the two loading points, or the existence of cracks at 45° between loading plates and supports. One can identify the horizontal cracks at the level of longitudinal reinforcements, which indicate shear failure.

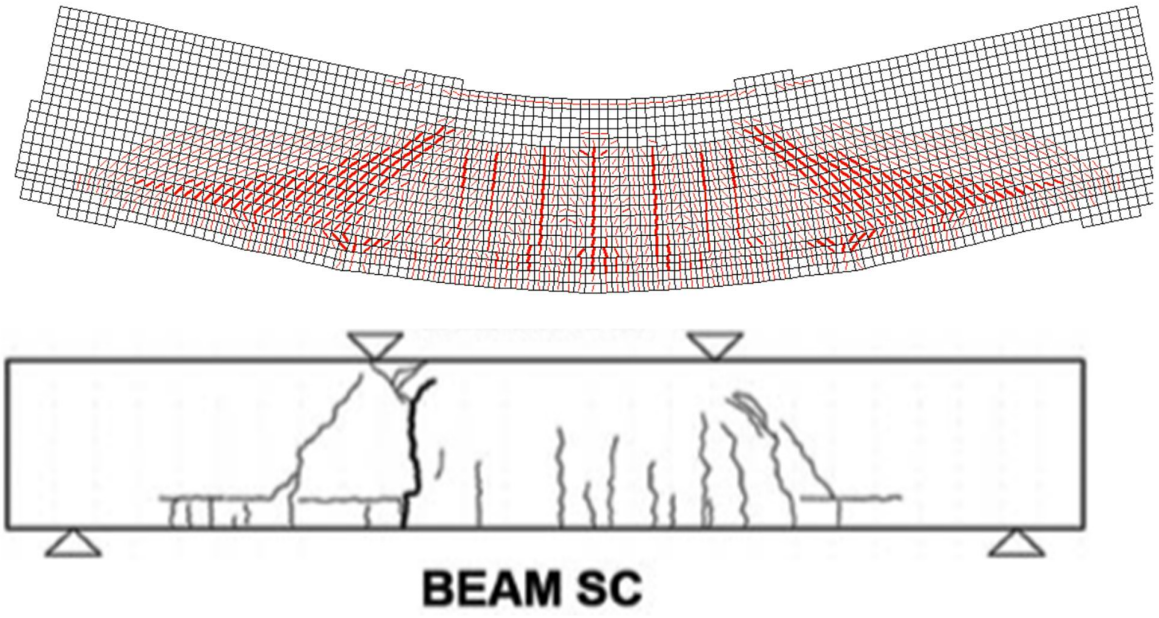

Figure 32 Comparison of crack patterns at failure load between FE model and experiment

Figure 33 shows the measured and predicted load-deflection curves of Beam SC. The first observation is that the FEM overestimates the stiffness of the beam. This can happen due to material imperfections and use of lower quality aggregates during the experiment. It is also possible that support deformations occurred in the test while the supports in the model were rigid. The peak load is captured very well with a difference between experiment and FEM being only 5.2%.

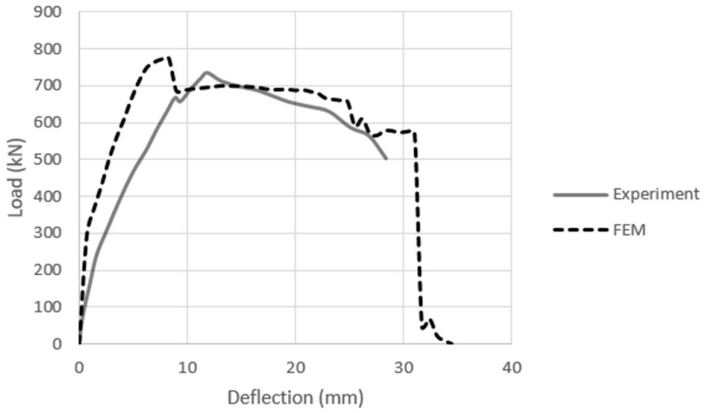

Figure 33 Load-deflection curve of Beam SC

The observations made regarding Beam SC are a good description of the comparisons made between experimental and FEM results. In each of the beams a high stiffness was noticed in the FEM, mainly due to perfect conditions imposed by the software. Every FEM beam failed with the critical crack forming in the middle of the beam. An exception was the control specimen which failed in shear.

Lastly, Figure 34 shows the failure loads of the four beams tested by Meda et al (2014). The FE software captured with good accuracy the failure loads of each beam, having an average error of 6.5%. As expected beams, SB and SC which had 50 mm of UHPFRC layers both on their bottom and side sides, produced the highest strengths. The increase in strength with respect to the reference beam SR was of 68%, and 71%, respectively.

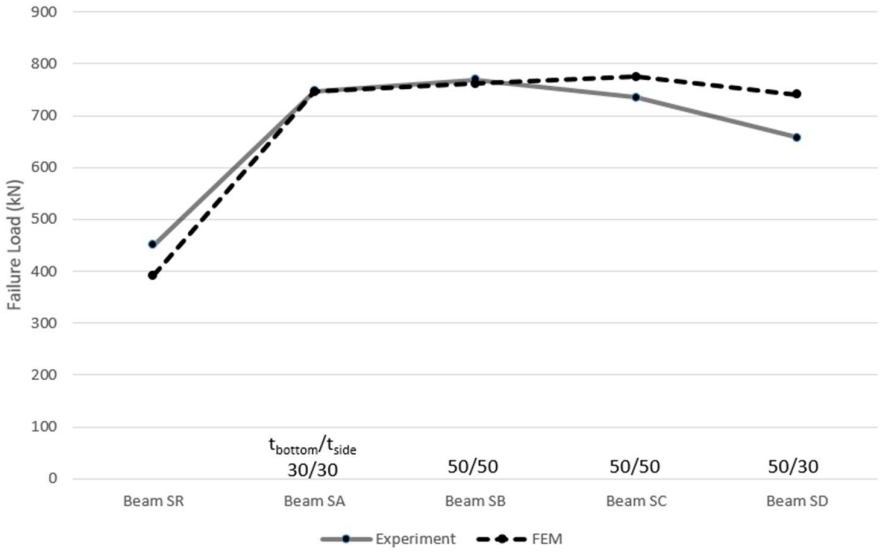

Figure 34 Failure loads for Meda et al series

Tests by Martinola et al. (2010)

In the following paragraph results from UHPCB beam will be discussed in detail. As seen in Figure 35, it is the beam reinforced with internal longitudinal and shear reinforcement, and retrofitted with 40 mm thick UHPFRC layers on bottom and side sides.

As shown in Figure 36, the predicted crack patterns of the beam are compared to the measured pattern at failure. The FEM captures very well the behavior of the experimental beam at failure load. In both cases the critical crack appears next to the left loading point. It indicates flexural failure with localization of stresses. This observation is attested by the FEM, where the longitudinal reinforcement yields at the given moment and the fibers are pulled out of the UHPFRC layer. Also the smaller cracks appearing between the loading points in the experiment are well predicted by the FEM.

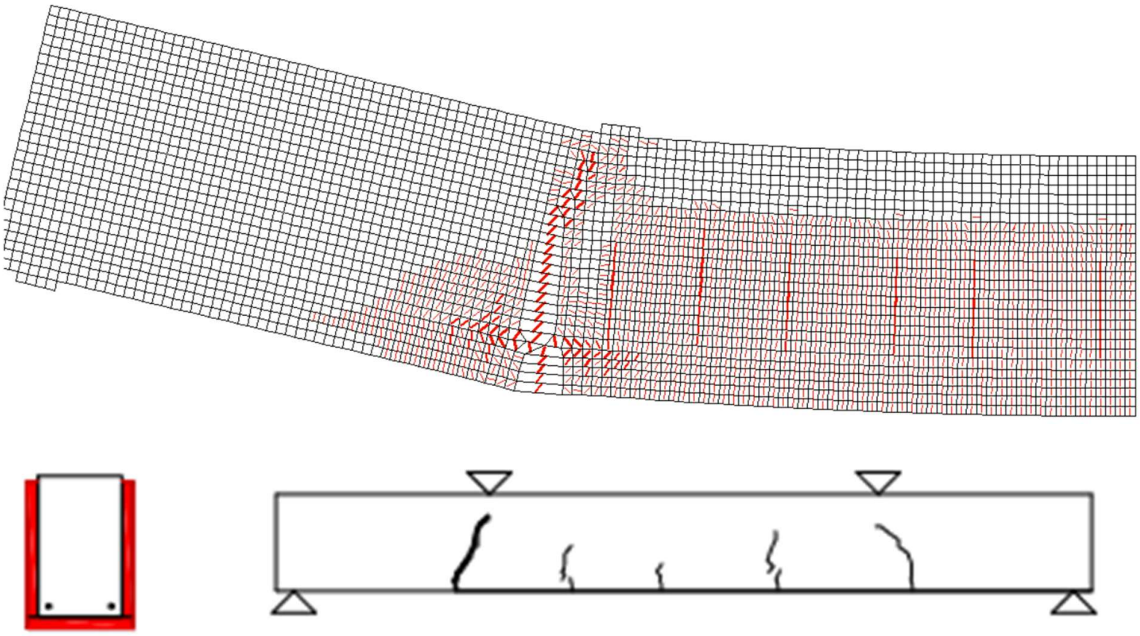

Figure 35 Comparison of crack patterns at failure load between FE model and experiment

Figure 37 shows the measured and predicted load-deflection curves of beam UHPCB. As it can be noticed, the FEM captures well the response up to failure load. At this point a sudden drop can be observed in FEM model, due to longitudinal reinforcement yielding and the fibers are pulled out in the UHPFRC layer. This is a great example of reduced ductility of UHPFRC retrofitted beam compared to the original beam. In the experiment the same drop was observed with the beam carrying more residual strength. The stiffness was overestimated due to absence of imperfections of the material in FEM.

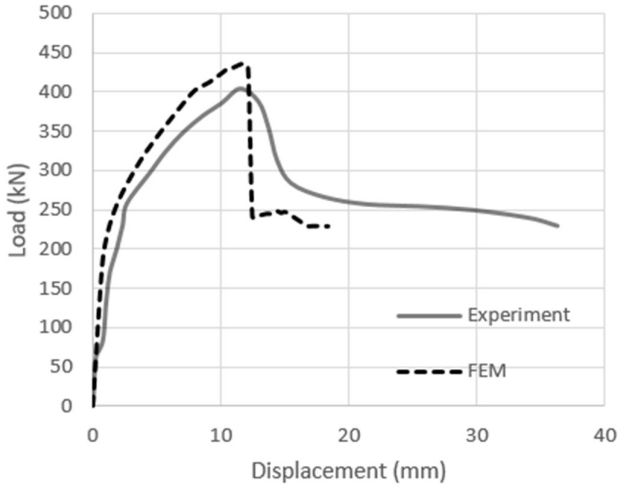

Figure 36 Load-deflection curve of beam UHPCB

Lastly, Figure 38 shows the failure loads of each beam. As it can be seen, for every test specimen the FE software overestimated the failure load. Nevertheless the average error is of an acceptable 6.5%. In case of UHPFC retrofitted beams a slight increase in error up to 10% can be seen, due to FE software working with ideal situations. As expected, the UHPFRC retrofitted beams exhibited greater resistance, than the normal concrete beam, with increase in strength of 212% between NCB and UHPCB for the experimental values and 221% in case of FEM analysis.

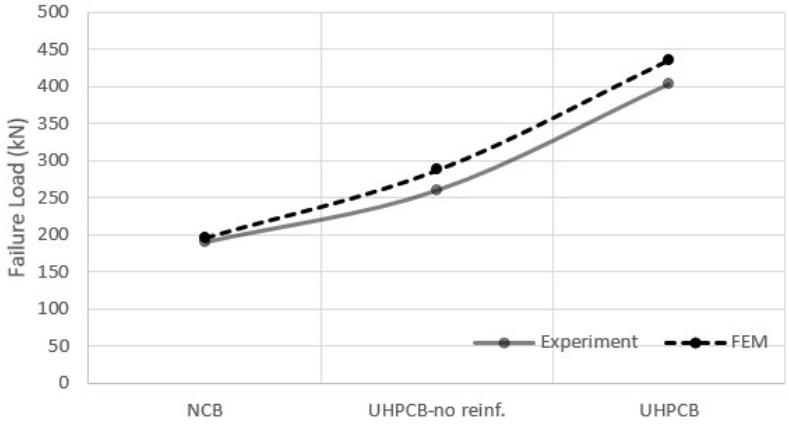

Figure 37 Failure load of beams for Martinola et al. series

It can be concluded, that in both Meda et al. and Martinola et al. series the FE software captures well the response described in the experiments, with a general tendency of overestimation of stiffness of specimens, due to absence of material imperfection in FEM.

5. Parametric study

In order to study the effect of FRP and UHPFRC retrofit on deep beams, a parametric study was carried out. Two parameters were studied in the case of FRP retrofit, namely span-to-depth ratio and FRP wrap configuration. For UHPFRC three variables were defined, namely span-to-depth ratio, fiber volume ratio and layer thickness. In the following chapter the models are descibed and results are discussed.

5.1. General data
FRP retrofitted beam

Figure 39 shows the geometrical properties of the beams from the parametric study. As one can see, some parameters are defined as variable. For these the values are as follows: shear span a= 1900mm, 3800mm or 5700mm; L= 4800mm, 8600mm or 12400mm; and n*FRP wrap which represents the number of FRP wraps on a beam. This varies from beam to beam, having configurations of width/spacing of 100mm/100mm, 100mm/200mm, 100mm/300mm or fully wrapped for each span-to-depth ratio case. Table 5 summarizes the remaining properties of the FRP-retrofitted beams from the parametric study.

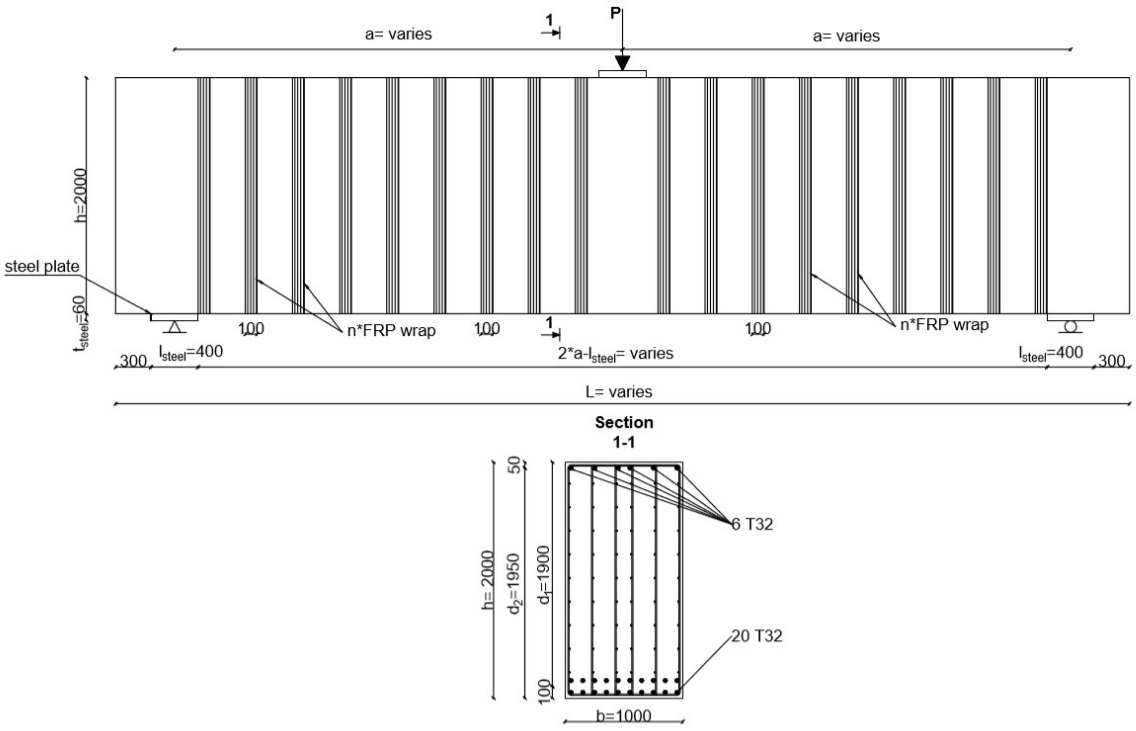

Figure 38 Geometrical parameters of beams retrofitted with FRP wraps

Table 5 Properties of beams retrofitted with FRP

							FRP wrap			
Beam name	$f_{yk\ b1,b2}$ [MPa]	$\rho_v=\rho_h$ [%]	$f_{yk\ v,h}$ [MPa]	f'_c [MPa]	a_g [mm]	E_c[GPa]	t [mm]	f_{yf} [MPa]	E_f [GPa]	esh [%]
CB-1	500	0.2	500	36	16	30	0.167	3800	234.5	1.7

where $f_{yk\ b1,b2}$= yield strength of longitudinal bars; ρ_v,ρ_h= vertical and horizontal shear reinforcement ratio; $f_{yk\ v,h}$= yield strength of shear reinforcement; f'_c= normal concrete cylinder strength; a_g= maximum aggregate size; E_c= Young's modulus of concrete; t= thickness of one FRP sheet; f_{yf} = yield tensile strength of FRP sheet; E_f= Young's modulus of FRP sheet; esh= ultimate strain of FRP.

UHPFRC retrofitted beam

Figure 40 shows the geometrical properties of beams from the parametric study. As one can see, some parameters are defined as variable. For these the values are as follows: shear span a= 1900mm, 3800mm or 5700mm, L= 4800mm, 8600mm or 12400mm,UHPFRC layer thickness t_{UHPFRC}= 50mm or 100mm; A final parameter, namely the fiber volume ratio has the given values V_f= 1, 2 or 3%. Table 6 summarizes the remaining properties of UHPFRC-retrofitted beams from the parametric study.

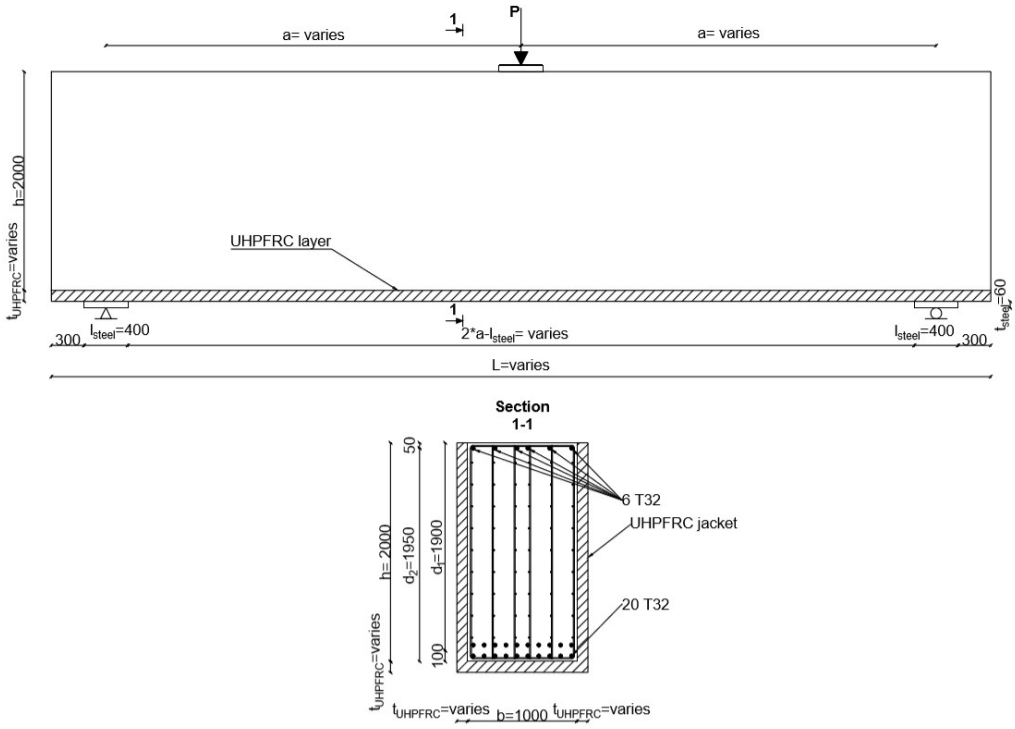

Figure 39 Geometrical parameters of beams retrofitted with UHPFRC layers

Table 6 Properties of beams retrofitted with UHPFRC

							UHPFRC			Fibers			
Beam name	$f_{yk\ b1,b2}$ [MPa]	$\rho_v=\rho_h$ [%]	$f_{yk\ v,h}$ [MPa]	f'_c [MPa]	a_g [mm]	E_c[GPa]	$f'_{c,jacket}$ [MPa]	$a_{g,jacket}$ [MPa]	E_{jacket} [GPa]	Type	L_f [mm]	Φ_f [mm]	f_{uf} [MPa]
CB-1	500	0.2	500	36	16	30	160	1	50	straight	20	0.35	2000

where $f_{yk\ b1,b2}$= yield strength of longitudinal bars; ρ_v,ρ_h= vertical and horizontal shear reinforcement ratio; $f_{yk\ v,h}$= yield strength of shear reinforcement; f'_c= normal concrete cylinder strength; a_g= maximum aggregate size of normal concrete; E_c= Young's modulus of normal concrete; $f'_{c,jacket}$= cylinder strength of UHPFRC jacket $a_{g,jacket}$= maximum aggregate size of UHPFRC jacket; E_{jacket}= Young's modulus of UHPFRC jacket.

The fiber characteristics are as follows: straight steel fibers with length of fiber L_f=20 mm; diameter of fiber Φ_f=0.35 mm; fiber ultimate tensile strength f_{uf}=2000 MPa.

5.2. Finite element models

5.2.1. FRP-retrofitted beams

In Figure 41 one can see the finite element model of beam FRPB-2-pw-100-200 built in program VecTor2. It has a span-to-depth ratio equal to two, and is wrapped with FRP strips of 100mm width with spacing of 200mm between them. The experimental specimens were modelled as half-beams, thus compilation time was greatly reduced. One roller was positioned at the end of the beam, while several others were installed in the place where the middle of the beam is in reality. Thus the whole system acts like a simple supported beam, and continuity of beam in the middle is not compromised.

Several displacements of 100 mm were placed on the loading plate at the top of the beam in order to capture the post-peak behavior of the beam. Steel plates were placed over the support and under the load to prevent concrete crushing.

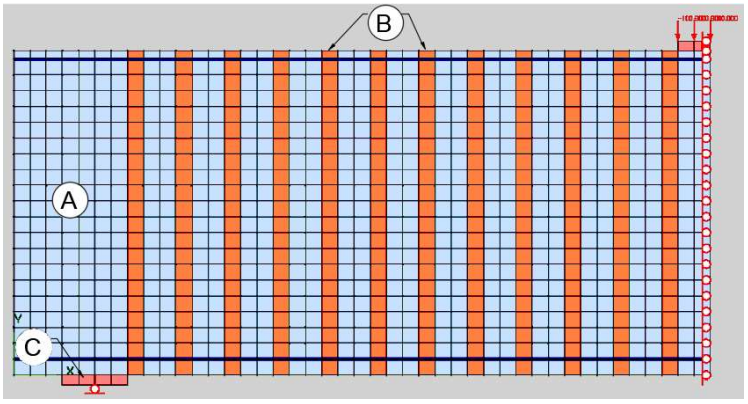

Figure 40 Finite element model of beam FRPB-2-pw-100-200

The FEM consists of two types of finite elements: quadrilateral elements, used for the modelling of concrete and steel plates, and truss elements used for the longitudinal reinforcement. A perfect bond is defined between the longitudinal reinforcement and the

surrounding concrete, as well as between the concrete and retrofitting material. The mesh size used in the model for quadrilateral elements is of 100x00 mm.

Material A represents the normal concrete. Its main characteristics are the cylinder compressive strength f'_c=22 MPa, the maximum aggregate size a_g= 16mm and Young's modulus E_c=30 GPa. Shear reinforcement is given as smeared reinforcement and has a ratio of 0.2% both in horizontal and vertical directions.

Material B represents the concrete part of the beam, which was retrofitted with the CFRP sheets. It has the same concrete properties as material B, with the addition of two CFRP sheets on each side as smeared reinforcement. This CFRP layer is characterized by its total thickness t=0.668 mm, tensile strength f_{yf}= 3800 MPa, Young's modulus E_f=234.5 GPa and a maximum elongation of 1.7%.

Material C represents the steel plates, having a yield strength f_y= 500 MPa.

5.2.2. UHPFRC-retrofitted beam

Figure 42 shows the finite element model of beam UHPFRCB-2-100-1 built in program VecTor2.

It has a span-to-depth ratio of 2, retrofitted with a 100 mm UHPFRC jacket having 1% fiber volume ratio. The experimental specimens were modelled as half-beams, in order to reduce compilation time and because the FE software can work with a maximum number of 10.000 finite elements. One roller was positioned at the end of the beam, while several others were installed in the place where the middle of the beam is in reality. Thus the whole system acts like a simple supported beam, and continuity of beam in the middle is not compromised.

Several displacements of 100 mm were placed on the loading plate at the top of the beam in order to capture the post-peak behavior of the beam. Steel plates (material C) were placed in both support and load points.

The FEM consists of two types of finite elements: quadrilateral elements, used for the modelling of concrete and steel plates, and truss elements used for the longitudinal reinforcement. A perfect bond is defined between the longitudinal reinforcement and the surrounding concrete, as well as between the concrete and retrofitting material. The mesh size used in the model for quadrilateral elements is of 100x100 mm.

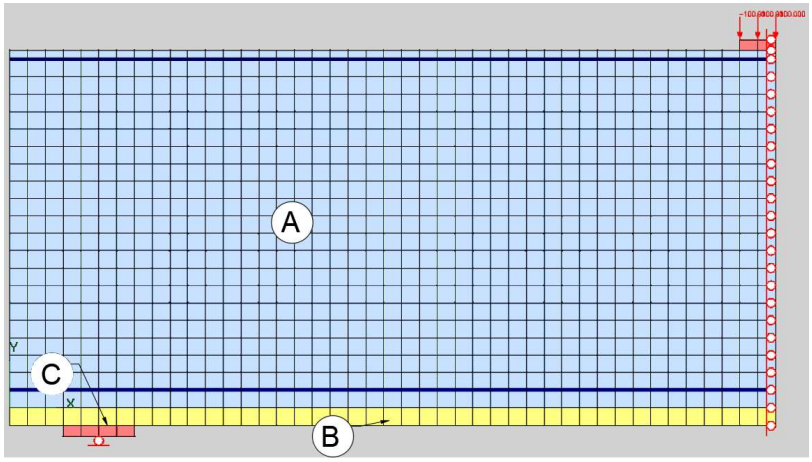

Figure 41 Finite element model of beam UHPFRCB-2-100-1

Material A represents the normal concrete. Its main characteristics are the cylinder compressive strength f'_c=22 MPa, the maximum aggregate size a_g= 16mm and Young's modulus E_c=30 GPa. Shear reinforcement is given as smeared reinforcement and has a ratio of 0.2% both in horizontal and vertical directions.

Material B represents the UHPFRC jacket. It has a cylinder compressive strength $f'_{c,jacket}$=160 MPa, Young's Modulus E_{jacket}=50 GPa and a maximum aggregate size $a_{g,jacket}$= 1mm. It contains straight steel fibers with fiber volume ratio V_f= 1%, fiber length l_f=20 mm, fiber diameter Φ_f=0.35 mm, fiber ultimate tensile strength f_{uf}= 2000 MPa, and fiber bond strength T_u=9.5 MPa.

Material C represents the steel plates, having a yield strength f_y= 500 MPa.

Because program VecTor2 works in 2D, other two regions were defined parallel to the regions of Material A. These two regions represent the side UHPFRC layers and have the same characteristics as Material B.

5.3. Discussion of results

In this paragraph the test result from the parametric study are analyzed and discussed. A total of 33 beams were created, 3 were created as control beams for each span-to-depth ratio, 12 beams were retrofitted with FRP, and 18 with UHPFRC. Firstly, the FRP retrofit results are discussed.

5.3.1. FRP-retrofitted beams

In order to understand how FRP retrofit improves the behavior of beams, the crack pattern and load displacement curve of an FRP retrofitted beam model will be compared to those of the control specimen. For this discussion, models FRPB-1-pw-100-100 and CB-1 will be used as example.

In Figure 42 the crack patterns of the finite element models at failure load are presented. As it can be seen, the control beam behaves as the strut-and-tie model for deep beams describes it. The critical cracks appear at an angle of about 45°, thus pointing to shear failure of beam. Also near the loading plate concrete crushing can be observed. For the FRP retrofitted beam the cracks appear also at an angle close to 45°, but wider cracks are created between the FRP wraps. This phenomenon is due to the fact that in FE software the FRP is modelled as shear reinforcement, with no possibility of debonding. Concrete crushing near the load plate can be observed in the FRP retrofitted beam too.

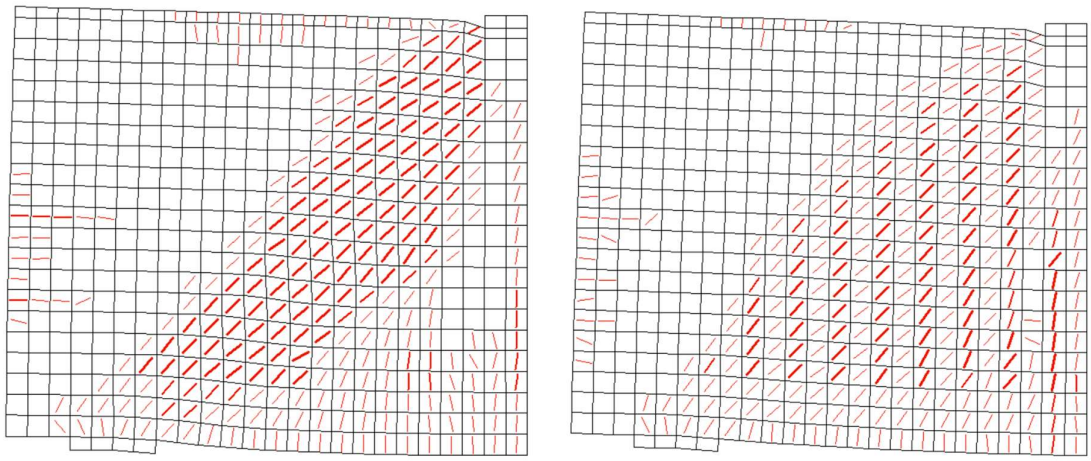

Figure 42 Comparison of crack patterns of FE models at failure load (CB-1 left, FRPB-1-pw-100-100 right)

Figure 43 shows the load-deflection curves of the two beams obtained from the finite element models. As it can be seen, at the first portion of the curve the stiffness is equal for both control beam and FRP retrofitted beam. At a 2mm deflection critical cracks start to appear in the models. While the stiffness of beam CB-1 starts to decrease, the slope of the FRPB-1-pw-100-100 curve continues almost unchanged. This trend continues until both beams reach failure load around the 8mm mark. In the end both beams fail in shear. The results show that a strength increase of 21% was achieved with FRP retrofit in the presented case.

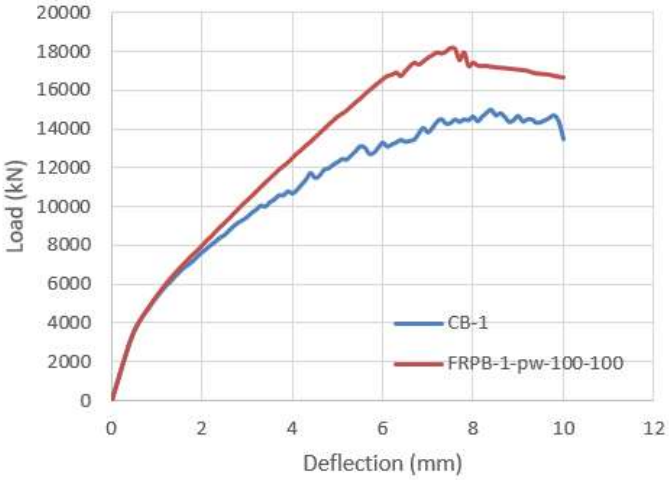

Figure 43 Load deflection curves of models CB-1 and FRPB-1-pw-100-100

As mentioned before, two parameters were used as variables in FRP retrofitted beams, namely shear-span-to-depth ratio and FRP configuration on beams. Firstly the shear-span-to-depth ratio will be discussed.

Figure 44 presents the effect of shear-span-to-depth ratio for two series, namely the control beams and the FRP whole wrap retrofitted beams (FRP-ww). As it can be noticed, the load capacity of the beams decreases as the a/d ratio increases. While for beams with a/d=1 the failure is due to shear, for more slender beams the failure turns into a flexural one.

Also it can be seen, that as the FRP wraps were placed perpendicularly to the horizontal axis, their effect is much greater for deeper beams. While for beams with a/d=1 the strength increase between control beam and FRP whole wrap retrofitted beam is of almost 30%, for beams with a/d=2 it is of 8% and for a/d=3 it has the value of 10%. The reason is that the slender beams failed in flexure.

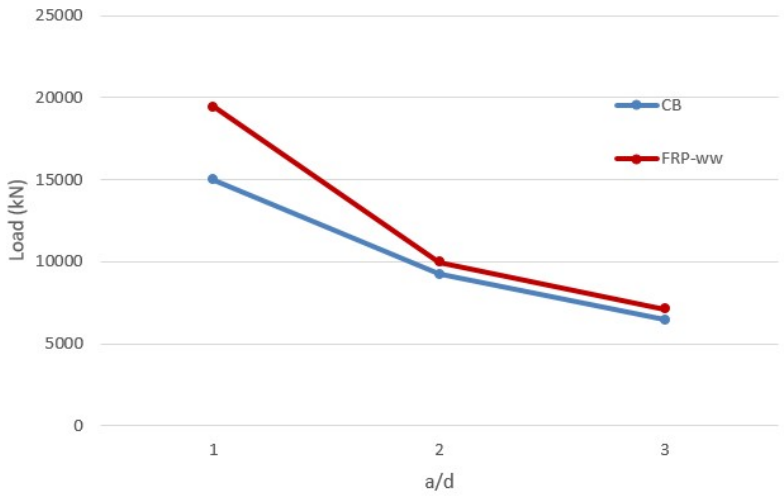

Figure 44 Effect of shear-span-to-depth ratio for CB and FRP-ww beams

Secondly, the effect of FRP configuration is discussed. For this part, the beams are separated in three categories, depending on their span-to-depth ratio. It is important to note that all beams were considered wrapped on all four sides.

In Figure 45 the effect of FRP configuration is seen for beams with different span-to depth ratios. For all beams the same thickness and type of FRP was used, only difference being between the surface area which they covered. The names pw and ww refer to partial wrap or whole wrap of surface of the beams. The numbers refer to the width of the FRP strips and the spacing between strips. For beam with a/d=1, also named deep beams, it can be seen that as more FRP strips are used in a denser configuration, higher failure loads are achieved. Strength increase from 12% in case of FRPB-1-pw-100-300 up to 30% in case of FRPB-1-ww can be

noticed with respect to the control beam CB-1. Also the cracks widths reduce in zones where FRP is applied.

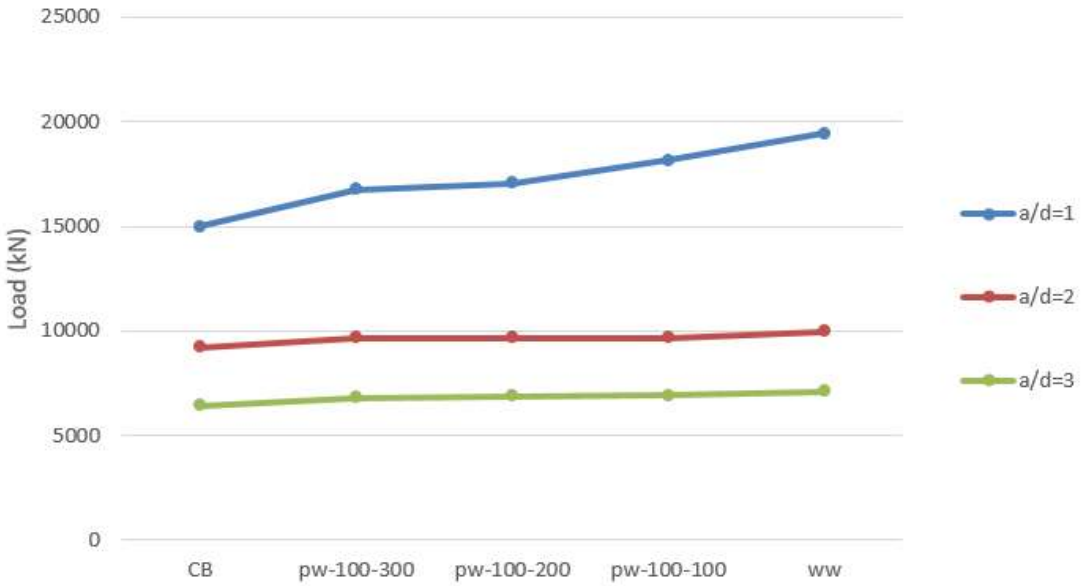

Figure 45 Effect of FRP configuration for beams with different a/d ratios

In case of beams with a/d=2, also named as medium beams, FRP retrofit does not have such a big impact on failure loads as in the previous case. This can be explained with the fact that all beams with a/d=2 started to fail in flexure. Nevertheless small strength increase from 4% in case of FRPB-2-pw-100-300 up to 8% in case of FRPB-2-ww is detected with respect to control beam CB-2.

Lastly, the effect of FRP configuration on so called slender beams with a/d=3 is discussed. For this series also the lack of major impact can be seen, due to the fact that beams are failing in flexure. Nevertheless strength increase is observed from 5% in case of FRPB-3-pw-100-300 up to 10% in case of FRPB-3-ww with respect to control beam CB-3.

5.3.2. UHPFRC-retrofitted beams

Firstly, just as in case of FRP retrofit, the crack patterns and load displacements curve of UHPFRC-retrofitted beam will be compared to the control specimen. For this discussion, models UHPFRCB-1-100-2% and CB-1 will be used as example.

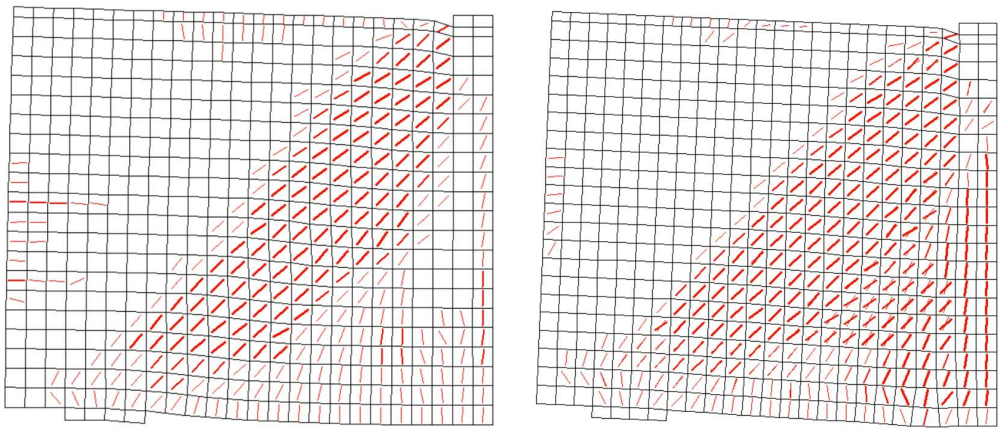

Figure 46 Comparison of crack patterns of FE models at failure load (CB-1 left, UHPFRCB-1-100-2% right)

In Figure 46 the crack patterns of the finite element models at failure load are presented. The control specimen behaves as mentioned before, with cracks appearing at an angle of about 45°, and failing in shear. As for the UHPFRC-retrofitted beam, a change in failure mode is noticed. As it can be seen, on the bottom part of the beam flexural cracks also appear. Indeed, from the load-displacement curve presented in Figure 49 it can be concluded that beam UHPFRCB-1-100-2% fails due to longitudinal reinforcement yielding, after which shear cracks also appear. Thus by retrofitting CB-1 with UHPFRC one can change the failure mode of the beam from shear failure to flexural failure.

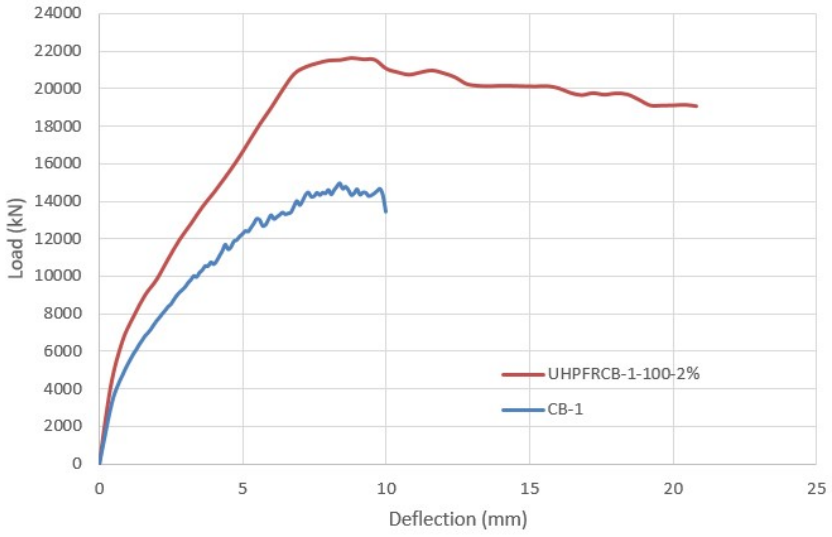

Figure 47 Load deflection curves of models CB-1 and UHPFRCB-1-100-2%

Figure 47 presents the load-deflection curves of the finite element models. As it can be noticed, in the control beam a stiffness softening phase appears due to appearance of larger cracks. The slope of the retrofitted beam on the other hand remains almost unchanged. This is due to the

fact, that the fibers inside the UHPFRC jacket start to work and restrain the opening of the cracks. The ultimate strengths of beams are reached at the almost the same displacement, indicating that the displacement capacity of the beam retrofitted with UHPFRC did not change with respect to the control specimen.

As mentioned before, while CB-1 fails in shear, UHPFRCB-1-100-2% fails due to flexure. The strength increase of the retrofitted beam is of 44% compared to the control specimen.

Firstly, the shear-span-to-depth ratio will be discussed.

Figure 48 presents the effect of shear-span-to-depth ratio for two beam series, namely the control beams and the UHPFRC-retrofitted beams which had 50mm-thick layers with 2% fiber volume ratio. As it can be noticed, the load capacity of the beams decreases as the a/d ratio increases. While for beams with a/d=1 the main failure mode is due to shear, for more slender beams the failure turns into flexural one.

Also the retrofit effect of UHPFRC layers decrease as the span-to-depth ratio increases. The explanation for this phenomena can be that in slenderer beams the longitudinal reinforcement reaches the yield strength before the full effect of UHPFRC layer could be exploited. This is confirmed by the strength increase for each a/d ratio. For a/d=1 a strength increase of 26% can be noticed between control beam and UHPFRC retrofitted one, while for a/d=2 the value is reduced to 15% and for beams with a/d=3 the value is of 8%.

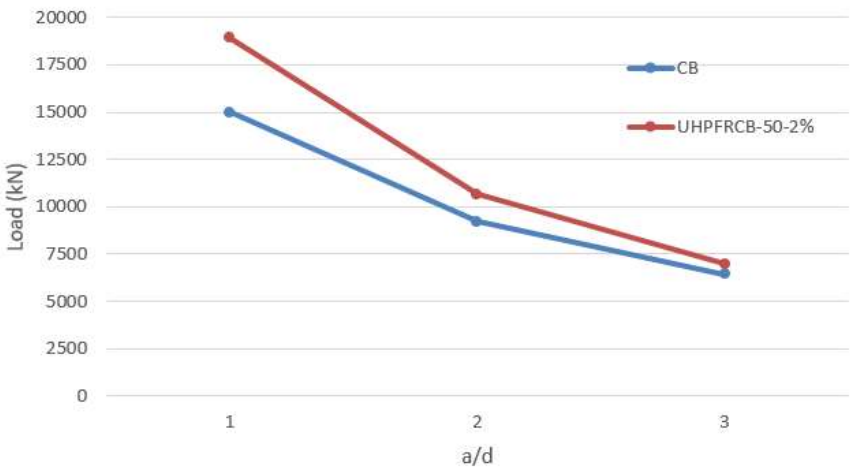

Figure 48 Effect of shear-span-to-depth ratio for CB and UHPFRCB-50-2% series

Secondly, in Figure 49 the effect of thickness of the layer is presented. As it can be seen, three set of beams are compared. For deep beams, with a/d=1 the impact of increasing layer thickness results in considerable strength increase. Strength increase from 33% in case of UHPFRCB-1-50-3% to 52% in case of UHPFRCB-100-3% with respect to control beam CB-1 can be observed. For medium beams (a/d=2) and slender beams (a/d=3) the effect is less impactful. Nevertheless an increase of strength from 18% to 27% with respect to control beam CB-2 can be observed for beams with a/d=2. In case of beams with a/d=3 the strength increase is from

10% to 18% with respect to control beam CB-3. It can be concluded that increasing UHPFRC layer thickness is more benefic for deeper beams than for slenderer ones.

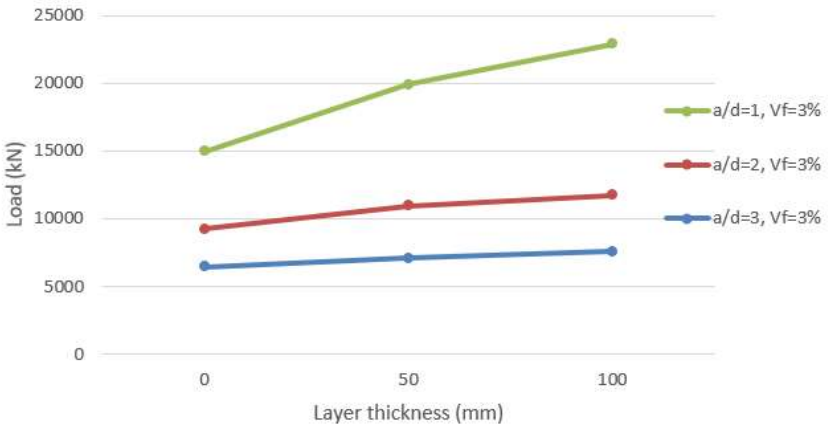

Figure 49 Effect of UHPFRC layer thickness

Lastly, the effect of fiber volume ratio is analyzed. For this part, the beams are separated in three categories, depending on their span-to-depth ratio.

Figure 50 shows the effect of fiber volume ratio for beams with a/d=1, also called deep beams. As it can be seen, for both 50mm and 100mm layer thicknesses the increase of fiber volume ratio induces increase in strength. An increase from 22% in case of UHPFRCB-1-50-1% up to 33% in case of UHPFRCB-1-50-3% with respect to CB-1 can be noticed for UHPFRC beams retrofitted with 50mm thick layers. The same growth with respect to CB-1 in case of 100mm layer thickness is from 35% in case of UHPFRCB-1-100-1% up to 53% increase for UHPFRCB-1-100-3%. It can be concluded that addition of more fibers from V_f=1% to 3% has a positive effect on strength of UHPFRC retrofitted.

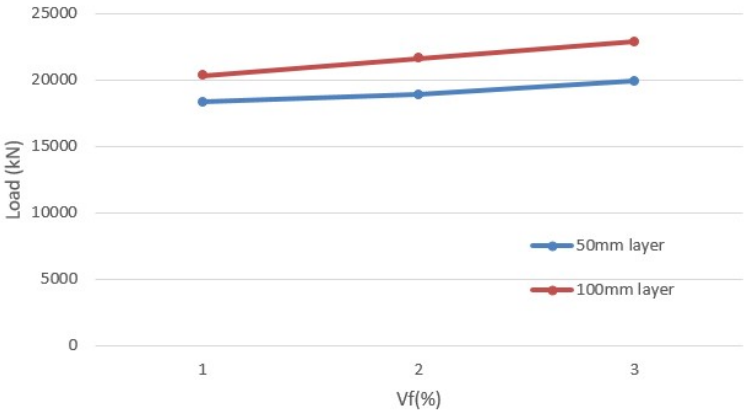

Figure 50 Effect of fiber volume ratio for deep beams (a/d=1)

In Figure 51 the effect of fiber volume ratio can be seen for medium beams (a/d=2). For this series also a strength of increase can be seen with addition of fibers to UHPFRC layers. Nevertheless the increase with respect to CB-2 is reduced, from 10% up to 18% in case 50mm UHPFRC layer thickness and from 21% up to 27% in case of 100mm UHPFRC layer thickness.

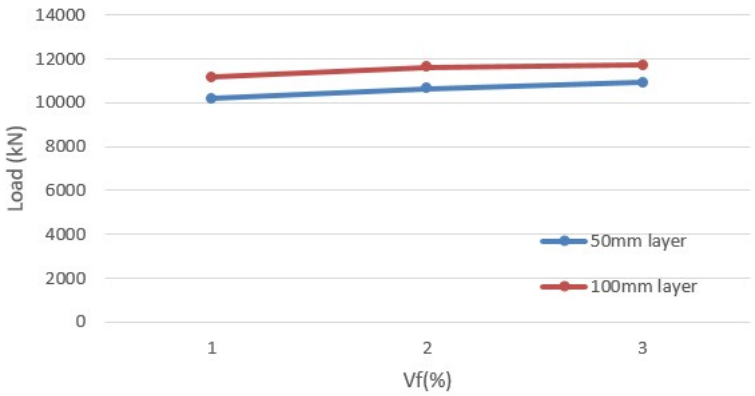

Figure 51 Effect of fiber volume ratio for medium beams (a/d=2)

Lastly, in Figure 52 the effect of fiber volume ratio on so called slender beams with a/d=3 is displayed. For this series also reduced impact can be seen, due to the fact that beams are failing in flexure. Nevertheless strength increase with respect to CB-3 is observed from 5% up to 10% in case of 50mm UHPFRC layer thickness and from 10% up to 17% in case of 100mm UHPFRC layer thickness.

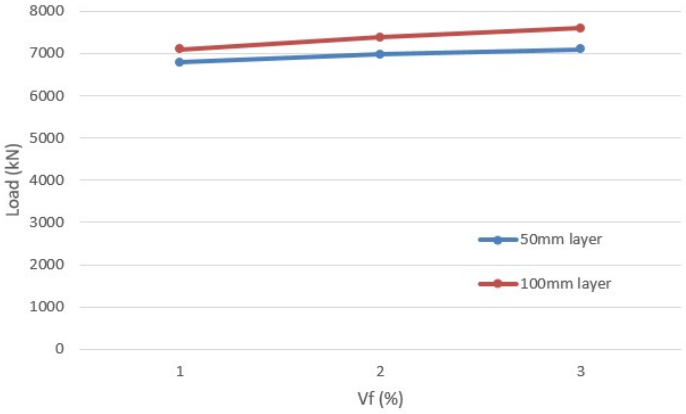

Figure 52 Effect of fiber volume ratio for slender beams (a/d=3)

5.3.3. Comparison of FRP and UHPFRC retrofit

Figure 53 shows the load-deflection curves of FRP and UHPFRC retrofit for deep beams (a/d=1). For this analysis the best retrofit methods from both FRP and UHPFRC are taken and compared. As mentioned before, both retrofit methods increase stiffness of beams up to failure load. It is very important to notice how FRP whole wrap retrofit and 50mm thick UHPFRC jacket retrofit have almost identical curves prior to load failure. This shows that on one hand for the presented parametric study UHPFRC retrofitting does not cause loss of ductility of element, and on second hand FRP retrofit can be as effective as UHPFRC if applied on whole surface of the beam. As it can be seen, 100mm thick UHPFRC jacket retrofit has the greatest impact on both stiffness and load capacity of beams. Neither in this case loss of ductility can be observed.

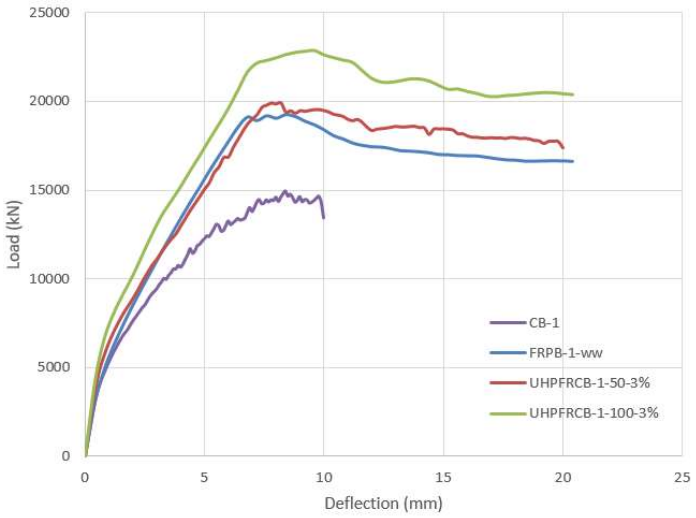

Figure 53 Load-deflection curves of FRP and UHPFRC retrofit for deep beams (a/d=1)

In Figure 54 the load-deflection curves of FRP and UHPFRC retrofit for medium beams (a/d=2) are presented. As before, best retrofit methods from both FRP and UHPFRC are taken and compared. In case of beams with a/d=2 the same remarks can be said as before. Nevertheless what can be noticed is a loss of ductility of beams, as retrofit methods are applied. All retrofitted specimens reach failure load at less deflection than the control specimen. Same remarks can be made about FRP whole wrap retrofit and 50mm thick UHPFRC jacket retrofit as before, with the difference being the not so effective increase of strength with respect to control beam. As mentioned before, this is caused by longitudinal reinforcement yielding prior to full exploitation of FRP and UHPFRC retrofits.

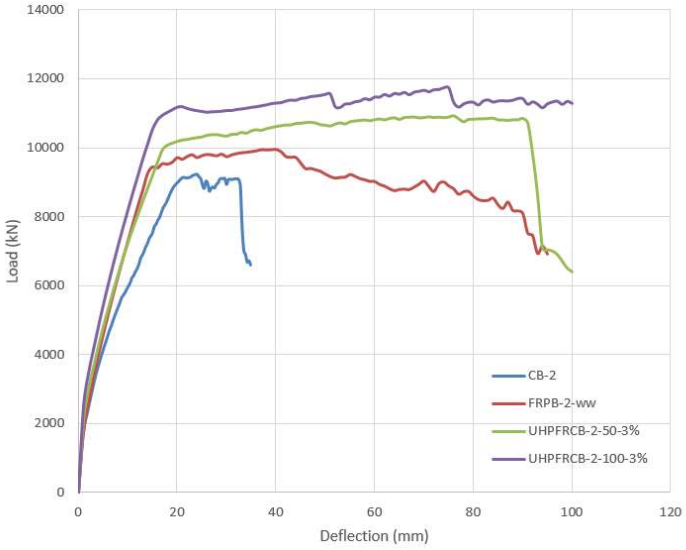

Figure 54 Load-deflection curves of FRP and UHPFRC retrofit for medium beams (a/d=2)

Lastly, in figure 55 the load-deflection curves of FRP and UHPFRC retrofit for slender beams (a/d=3) are shown. All remarks made at medium beams are true in case of slender beams also.

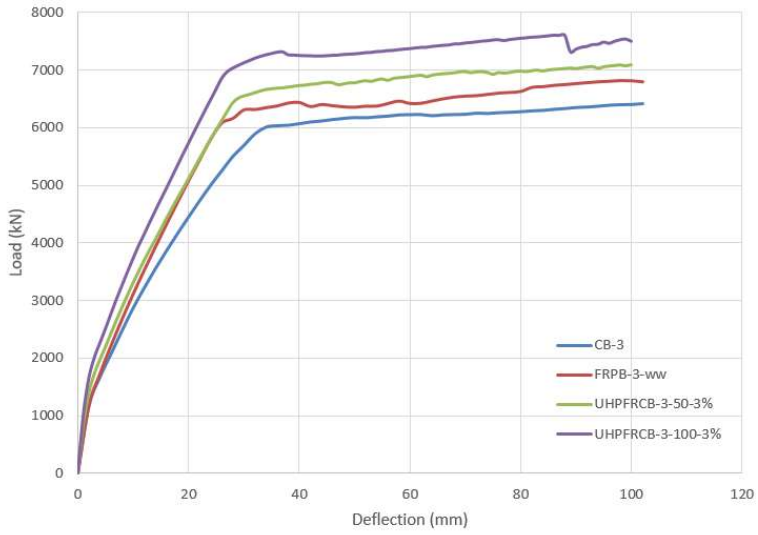

Figure 55 Load-deflection curves of FRP and UHPFRC retrofit for slender beams (a/d=3)

When comparing FRP retrofit with UHPFRC retrofit for deep beams, one must consider several variables. Besides strength enhancement criteria there is the financial influence, the environmental conditions etc. Important to note that every retrofitting case differs from one another and has to be treated in a separate manner.

In this last part of comparison the advantages of each retrofit technique are presented.

FRP retrofit advantages:

- FRP sheets are much lighter than UHPFRC jacketing. Thus the structure is not loaded with considerable extra weight
- FRP retrofit layer is much thinner than UHPFRC layer
- Fiber efficiency can be maximized for FRP retrofit whereas in UHPFRC layers fiber orientation is random.
- Even though both retrofit material have high costs, FRP retrofitting cost less than UHPFRC retrofitting

UHPFRC retrofit advantages:

- UHPFRC layers work well in both tension and compression, whereas FRP sheets work only in tension
- Unlike FRP sheets, UHPFRC jackets withstand high temperatures, thus not needing protection against fire.
- UHPFRC retrofit withstands hars environmental conditions such as salty water or even chemical degradation (chlorine).
- UHPFRC retrofitted structure is very durable and has longer service life than FRP retrofitted one.
- UHPFRC retrofit can be applied with great success to rough surfaces also, unlike FRP sheets.
- If applied correctly, debonding cannot occur for UHPFRC layers, unlike FRP ones.

6. Summary and conclusions

The main goal of this thesis was to use advanced nonlinear finite element models in order to understand the behavior of deep beams retrofitted with FRP sheets and UHPFRC layers. The nonlinear analyses were performed based on the Modified Compression Field Theory which is a smeared rotating crack approach implemented in program VecTor2.

The first part of the thesis consisted of gathering and summarizing information about the properties, advantages and disadvantages of FRP sheets and UHPFRC materials when used for the retrofit of existing structures. The Modified Compression Field Theory was also studies and summarized to provide background for the following analyses.

The second part of the thesis focused on the modelling of tests of FRP- and UHPFRP retrofitted deep beams from the literature. A total of four tests were collected and studied in order to understand the effect of the test variables. The predictions of the finite element models were compared to the test results in order to validate the models and to further understand the behavior of the test specimens.

Finally, the validated model was used to perform parametrical studies to investigate the effect of FRP sheets and UHPFRC layers on the behavior of true-scale deep beams. The variables investigated in a systematic manner included the aspect ratio of the member, the layout of the FRP sheets, the thickness and fiber content of the UHPFRC layers. The results were used to compare the effectiveness of the two retrofitting techniques.

Based on these investigations, the following main conclusions were reached:

- The finite element model based on the Modified Compression Field Theory captures well the complete behavior of FRP-retrofitted deep beams tested in the structural laboratory. Exceptions to this observation were beams in which the FRP sheets were not applied to the entire depth of the section and exhibited early debonding.
- It was shown that early debonding can be estimated reasonably well by imposing a limit on the strains in FRP sheets. The nonlinear analyses were terminated when the strain reached the limit value recommended in American design code ACI 440.2R-08.
- As UHPFRC-retrofitted test specimens did not exhibit delamination of the UHPFRC layers, the nonlinear finite element model captured well the behavior of all studied deep beams. This included agreement in terms of load-deflection response, crack patterns and failure modes. It was however noted the models produced slightly higher stiffness that observed.
- The parametric study demonstrated that both FRP and UHPFRC retrofitting strategies have beneficial effect on the shear strengths of deep beams. Strength increase of up to 30% in case of FRP-retrofitting strategy was observed, while for UHPFRC-retrofitting strategy the value was 53%. A favourable effect in terms of ductility was observed when the UHPFRC layers changed the failure mode from shear to flexural.

Finally, this work resulted in several ideas for future research on the topic of FRP and UHPFRC-retrofit of deep beams. It is noted that there is a need to integrate the debonding of the FRP sheets in the finite element analysis in a more consistent manner. Furthermore, while this thesis focused mostly on the strength of the members, it is also of interest to study the effect of retrofitting on the service behavior in terms of crack and deflections. Finally, while the finite element approach can provide adequate predictions, it is too complex and time consuming to be used on a daily basis. Therefore, it is necessary to develop simpler rational models that are capable of capturing the effect of FRP sheets and UHPHRC layers applied on existing deep beams.

References

ACI Committee 440, 2008. "Guide for the Design and Construction of Externally Bonded FRP Systems for Strengthening Concrete Structures", American Concrete Institute, Farmington Hills, MI

Bukhari, I.A., Vollum, R., Ahmad, S., Sagaseta, J., 2013, "Shear Strengthening of Short Span Reinforced Concrete Beams with CFRP Sheets", Arab J Sci Eng

Da Silva. W.R.L., Svec, O., Thrane, L.N., Pade, C., 2017, "Effect of fibre orientation on the tensile strength of ultra-high performance steel fibre-reinforced self-compacting concrete", AFGC-ACI-fib-RILEM Int. Symposium on Ultra-High-Performance Fibre-Reinforced Concrete, Montpellier, France

Denarie, E., Jacomo, D., Fady, N., Corvez, D., 2013, "Rejuvenation of maritime signalization structures with UHPFRC", AFGC-ACI-fib-RILEM Int. Symposium on Ultra-High-Performance Fibre-Reinforced Concrete, Marseille, France

European Committee for Standardization: EN 1992-1-1 Eurocode 2, 2004, "Design of Concrete Structures - Part 1-1: General Rules and Rules for Buildings", CEN, Brussels.

fib Task-group 9.3, 2001, "Externally Bonded FRP Reinforcement for RC Structures" International Federation for Structural Concrete, fib Bulletin 14, pp 1-138.

FRP products: http://www.mpnc.net.au/fibre-reinforced-polymer/ ;
http://www.zacarbon.com/cfrp-rebar; http://basalt.today/images/netcr63_03-7.pdf

https://en.wikipedia.org/wiki/Girder_bridge#/media/File:Dunn_Memorial_Bridge_stub_end.jpg

Lee,S.-C.,Cho,J.-Y.,Vecchio,F.J.,2011,"Diverse Embedment Model for Steel Fiber-Reinforced Concrete in Tension: Model Development", ACI Materials Journal, Vol. 108, No.5, pp. 516-525.

Lee,S.-C.,Cho,J.-Y.,Vecchio,F.J.,2011,"Diverse Embedment Model for Steel Fiber-Reinforced Concrete in Tension: Model Verification", ACI Materials Journal, Vol. 108, No.5, pp. 526-535.

Lee, S.-C., Cho, J.-Y., Vecchio, F.J., 2013, "Tension-Stiffening Model for Steel Fiber-Reinforced Concrete Containing Conventional Reinforcement", ACI Structural Journal, Vol. 110, No.4, pp. 403-412.

Malek, A.M., Saadatmanesh, H., Ehsani, M.R., "1998, Prediction of Failure Load of R/C Beams Strengthened with FRP Plate Due to Stress Concentration at the Plate End" ACI Structural Journal, Vol. 95, No. 1, pp. 142-152,

Martinola, G., Meda, A., Plizzari, G.A., Rinaldi, Z., 2010, "Strengthening and repair of RC beams with fiber reinforced concrete", Journal: Cement & Concrete Composites

Matthys, S., 2010, “Structural behaviour and design of concrete members strengthened with externally bonded FRP reinforcement” Doctoral Thesis, Department of Structural Engineering, Ghent University, Ghent, Belgium, 59 p.

Meda, A., Mostosi, S., Riva, P.,2014, “Shear Strengthening of Reinforced Concrete Beam with High-Performance Fiber-Reinforced Cementitious Composite Jacketing”, ACI Structural Journal, Title No. 111-S89

Moreillon, L., Menetrey, P., 2013, “Rehabilitation and strengthening of existing RC structures with UHPFRC: various applications”, AFGC-ACI-fib-RILEM Int. Symposium on Ultra-High-Performance Fibre-Reinforced Concrete, Marseille, France

Naaman, A.E., 2007, “HIGH PERFORMANCE FIBER REINFORCED CEMENT COMPOSITES: CLASSIFICATION AND APPLICATIONS.”

Nie, J. G., W. H.Pan, M. X.Tao, and Y. Z. Zhu, 2017, “Experimental and numerical investigations of composite frames with innovative composite transfer beams.” J. Struct. Eng. 143

Rasheed, M.M., 2016, “Retrofit of Reinforced Concrete Deep Beams with Different Shear Reinforcement by Using CFRP”, Civil and Environmental Research, Vol.8, No.5

Riedel, P., Leutbecher, T., 2017, “Effect of specimen size on the compressive strength of ultra-high performance concrete”, AFGC-ACI-fib-RILEM Int. Symposium on Ultra-High-Performance Fibre-Reinforced Concrete, Montpellier, France

Shi, C., Mo, Y. L., 2008, “High-Performance Construction Materials- Science and Application”, Engineering Materials for Technological Needs – Vol.1, World Scientific Publishing Co. Pte. Ltd.

Tayeh, B.A., et al., 2013, “Utilization of ultra-high performance fibre concrete (UHPFC) for rehabilitation–a review” Procedia Engineering, 2013. 54: p. 525-538.

Wong, P., Trommels, H., Vecchio, F. J., 2013, “VecTor2 and FormWorks Manual”

Yu, R., Spiesz, P., J. H. Brouwers, H., 2015, “Development of Ultra-High Performance Fibre Reinforced Concrete (UHPFRC): Towards an efficient utilization of binders and fibres.” Construction and Building Materials. 79. 273-282.

Zani, G., Colombo, M., di Prisco, M., 2017, “Size effect of HPFRCC in uniaxial tension”, AFGC-ACI-fib-RILEM Int. Symposium on Ultra-High-Performance Fibre-Reinforced Concrete, Montpellier, France